International Journal of Hydrogen Energy 88 (2024) 1237–1255

Contents lists available at ScienceDirect

International Journal of Hydrogen Energy

journal homepage: www.elsevier.com/locate/he

Carbon-negative "emerald hydrogen" from electrified steam methane reforming of biogas: System integration and optimization

Andrea Nava [a], Davide Remondini [b], Stefano Campanari [a], Matteo C. Romano [a,*]

[a] Politecnico di Milano, Department of Energy, Via Lambruschini 4, 20156, Milan, Italy
[b] Snam S.p.A., San Donato Milanese, Milan, Italy

ARTICLE INFO

Keywords:
Biogas
Hydrogen
Electrified reforming
Renewable energy
CO_2 capture
Negative emission

ABSTRACT

This work assesses a chemical plant for the conversion of biogas into negative emission "emerald hydrogen" via electrified reforming and CO_2 separation. Electrification of the reformer allows for enhanced syngas production, compact reactor designs and flexible operation, thanks to the avoidance of combustion and heat transfer through pressure walls. The integration of the process with solar and wind power generation has been assessed by part-load process simulations and plant sizing and operation optimization through yearly simulations with hourly discretization. Different European locations with different wind and solar availabilities were assessed considering (i) short- and long-term cost scenarios for renewables and battery technologies and (ii) different plant size (from 390 to 3900 Nm^3/h of biogas capacity). The overarching scope of the paper is to calculate the cost of the produced hydrogen and the economic value of flexibility for plants installed in different locations, under different cost scenarios.

At design load, the assessed process consumes 17.7 kWh of electricity per kg_{H2} and retains 96% of the biogas chemical energy in the produced hydrogen. Additionally, 76% of the biogenic carbon is recovered as high-purity liquid CO_2, achieving up to −9 kg_{CO2}/kg_{H2} negative emissions.

When powered with 95% of renewable energy, hydrogen production cost ranges from 2.5 to 2.9 €/kg for a long-term REN cost scenario and large-scale flexible plant to 5.9–7.1 €/kg for a short-term REN cost scenario and small-scale inflexible plants. For small-scale plants, flexibility allows to reduce the hydrogen production cost by 11–16% with respect to the inflexible plant in the short-term renewables cost scenario and by 1–4% in the long-term cost scenario. For large-scale plants, the adoption of a flexible plant leads to a reduction of 17–23% of the hydrogen cost in the short-term scenario and of 6–22% in the long-term scenario.

Nomenclature

bcm	Billion cubic metres
BESS	Battery Energy Storage System
CAPEX	CAPital EXpenditure
CCR	Carbon Capture Ratio
CF	Capacity Factor of renewable sources
DoD	Depth of Discharge
eBGR	Electrified BioGas Reforming system
eSMR	Electrified Steam Methane Reformer
EE	Electric Energy
FTR	Fired Tubular Reformer
GS	Gas Separation
KPIs	Key Performance Indicators
LCOE	Levelized Cost Of Electricity
LHV	Lower Heating Value
MDEA	Methyl-Diethanolamine
Mt	Million tonnes
OPEX	OPerative EXpenditure
POCS	Periodic Open Cellular Structure
PSA	Pressure Swing Adsorption
REN	Renewable energy
RENS	Renewable Energy Share
SG	Syngas Generation
SMR	Steam Methane Reforming
SOC	State Of Charge
WGS	Water Gas Shift

(*continued on next column*)

(*continued*)

* Corresponding author.
E-mail addresses: andrea.nava@polimi.it (A. Nava), matteo.romano@polimi.it (M.C. Romano).

https://doi.org/10.1016/j.ijhydene.2024.09.171
Received 26 June 2024; Received in revised form 23 August 2024; Accepted 14 September 2024

1. Introduction

With a biogas and biomethane production of 21 bcm, Europe could have produced 28 Mt of biogenic CO_2 in 2022. Projections estimate this potential to grow to 46 Mt by 2030 and 124 Mt by 2050 (with a biogas and biomethane production of 35 and 95 bcm, respectively) [1–3]. Therefore, introducing processes for the production of decarbonised energy carriers from biogas with CO_2 capture and storage would allow to remove large amounts of CO_2 from the atmosphere and generate significant revenues from carbon credits.

Electrified steam methane reforming (eSMR) technology aligns with this goal, enabling efficient syngas production at small-scale with compact and flexible reactors design that can adapt to the intermittent nature of renewable energy sources. This approach intensifies the syngas generation process and reduces the loss of biogenic carbon as vented CO_2 (something to be avoided in carbon-constrained economies, where the high-value biogenic carbon should either be stored or used for the production of biofuels and biochemicals [4]).

An example of this technology was developed by Wismann et al. [5,6], in collaboration with *Topsoe*, resulting in the delivery of the *eREACT*^{TM} technology [7]. This eSMR unit is currently undergoing testing at the pilot plant situated at the Aarhus University biogas research facility [8]. Other research activities are focussing on improving the heat transfer properties of electrified reactors. For instance, utilizing a conductive structure such as foams or POCS (periodic open cellular structures) allows to enhance heat transfer properties, increasing reactor compactness and operational flexibility [9–12].

Broadly speaking, electrification of endothermic reactors facilitates the design of flexible reactors suitable for both small- and large-scale applications. These modular designs are versatile and can be employed for the production of various energy carriers through processes such as hydrocarbon cracking, methane pyrolysis, dry reforming, and reverse water-gas shift reactions [13,14].

A number of recent studies have investigated the production of hydrogen from biogas using conventional reforming technology. In this process, a portion of the biogas or an auxiliary fuel is combusted in order to support the endothermicity of the reactor. Montenegro et al. conducted an evaluation of the techno-economic performance of converting biogas into hydrogen using BioRobur technology, which is an autothermal biogas reforming reactor that combines steam methane reforming with catalytic partial oxidation. The cold gas efficiency of the process is 65% and hydrogen is produced at a cost between 2.7 and 5.3 €/kg_{H2}, depending on the capacity of system (700–50 Nm^3/h of hydrogen produced, respectively). These results were obtained by considering municipal solid waste as feed at zero cost and without CO_2 capture from the syngas [15].

Crispim et al. evaluated the economic feasibility of hydrogen production from biogas using conventional reforming technology, with municipal solid waste as the feedstock [16]. In their study, only 71% of the biogas was utilized in the reformer, while the remainder was used to sustain the process. The hydrogen yield relative to reformed CH_4 was reported as 0.34 kg_{H2}/kg_{CH4} [17] (corresponding to a cold gas efficiency of 80%). However, this analysis did not include a simulation of the chemical plant. Their evaluation of 28 landfills in the state of Minas (Brazil) found that the minimum cost of hydrogen production, with CO_2 capture, was approximately 7 US$/kg.

The work of Cormos et al. and Selejan et al. analysed large-scale biogas production (50′000 to 100′000 Nm^3/h of hydrogen produced) and evaluated different CO_2 capture technologies from the syngas. Cold gas efficiencies from 54% to 66% and a levelized hydrogen cost of between 1.75 and 2 €/kg_{H2} was found [18,19]. The competitive hydrogen cost results both from the very large plant capacity, hardly compatible with the capacity of biodigesters, leading to favourable economies of scale and sophisticated design such as heat recovery steam Rankine cycle, and from the assumed low biogas cost (4.6 €/GJ).

Madeira et al. simulated a hydrogen production process from biogas using a conventional reformer. In this case, 18% of the biogas was combusted within the process, and a cold gas efficiency of 79% was achieved, resulting in a production cost of 4.6 US$/$kg_{H2}$. This study did not incorporate thermal integration of the system nor CO_2 capture from the syngas [20].

Lachén et al. investigated the production of hydrogen from biogas using a two-zone fluidised bed reactor, with the integration of permselective metallic membranes (Pd/Ag) within the fluidised bed. Up to 68%

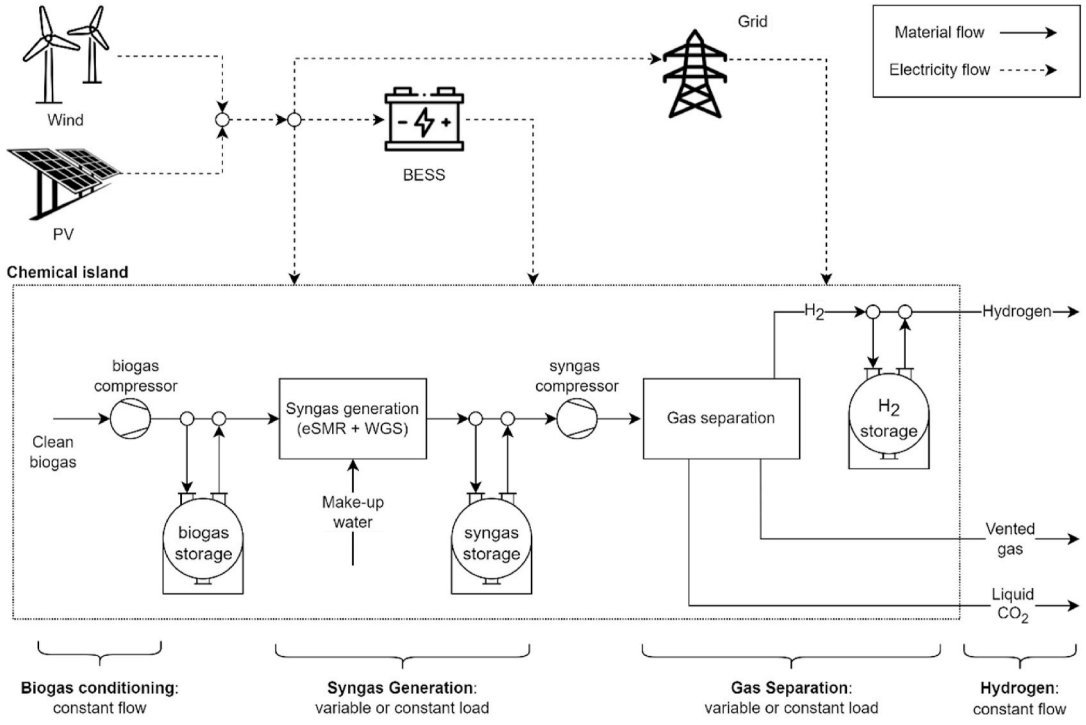

Fig. 1. Block diagram of the biogas to hydrogen process with power supply and storage systems.

cold gas efficiency was obtained by integrating this reactor with the steam-iron process. The calculated hydrogen production cost ranges between 4 and 15 €/kg without considering carbon capture [21].

Ongis et al. conducted a techno-economic analysis of a small-scale hydrogen production plant utilizing biogas and autothermal reformer technology with membranes. This approach enables the production of pure hydrogen from the reactor permeate, with up to 90% cold gas efficiency, at a cost of 4.4 €/kg [22].

To the best of the authors' knowledge, the only techno-economic analysis on biohydrogen production from electrified reforming is that of Maporti et al. Their simulation did not account for CO_2 capture from the syngas or thermal integration with the biodigester. The entire biogas stream feeds the reactor, achieving a hydrogen production efficiency of 95% relative to the biogas energy content. The hydrogen production cost ranged from 3 to 6 €/kg_{H2}, depending on electricity prices (ranging from 50 to 200 €/MWh) and biogas costs (ranging from 0.2 to 0.3 €/Nm^3) [23].

This study proposes a conversion pathway for the production of hydrogen from biogenic sources with CO_2 capture, which we name "emerald hydrogen". The process assessed in this work (Fig. 1) is designed to convert clean biogas into hydrogen through: (i) a syngas generation unit formed by an eSMR and a water gas shift (WGS) reactor; (ii) CO_2 separation with a solvent-based process; (iii) CO_2 liquefaction for transport by truck and (iv) hydrogen purification. The plant is conceived to be operated flexibly, adapting its load based on the availability of renewable electricity. Therefore, the plant is equipped with gas storage tanks for biogas, syngas and hydrogen, that allow to decouple the gas flow rate through the different sections of the plant, aiming at adapting the load of the electric intensive sections to the availability of renewable energy, while keeping a fixed inflow biogas flow rate and a fixed outflow hydrogen flow rate. The electricity to run the system is supplied by photovoltaic (PV) panels and wind turbines, assisted by a battery energy storage system (BESS) and electric grid connection for the management of their intermittency.

This work presents the first comprehensive techno-economic analysis of carbon-negative H_2 production from biogas with an electrified SMR system via: (i) process engineering study with the calculation of the mass and energy balances of the process at different loads with off-design model and (ii) rigorous economic optimization of the process integrated with photovoltaic and wind power generation system in different European locations, based on yearly simulations with hourly resolution. The overarching scope of the paper is to calculate the cost of the produced negative-emission "emerald hydrogen" and the economic value of flexibility for plants installed in different locations, under different cost scenarios.

2. System description

2.1. Chemical island

The system considered in this study exploits a 500 kg/h (390 Nm^3/h) of clean biogas with molar composition 55% CH_4 and 45% CO_2 and corresponding thermal power of 2.14 MW_{LHV}. This capacity is representative of typical biogas Italian plants for electricity generation.

Clean biogas (stream #1 in Fig. 2), is initially compressed to 9 bar and then feeds the bottom stage of a saturator, where the biogas rises

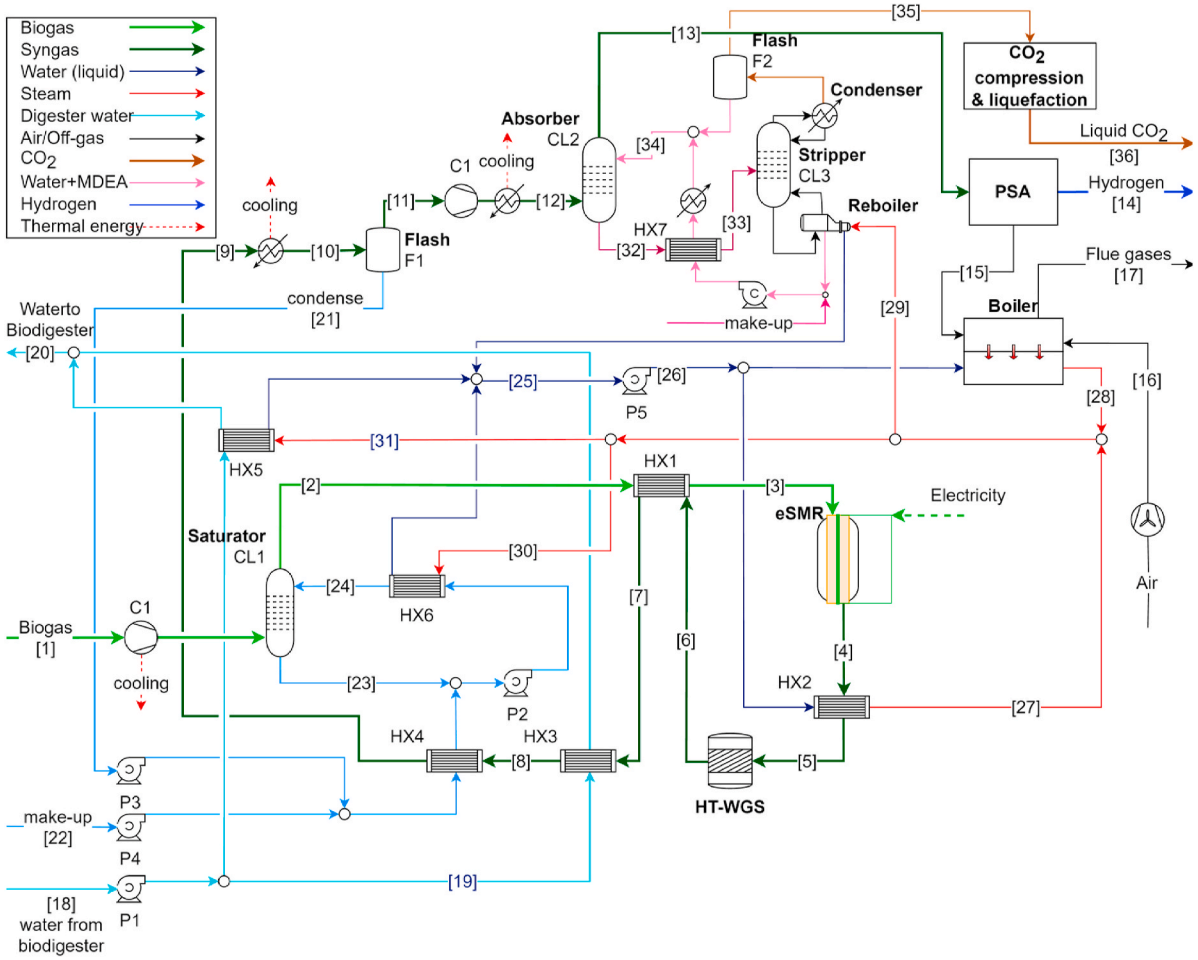

Fig. 2. Process flow diagram of the biogas to hydrogen plant based on electrified Biogas Reforming (eBGR).

toward the head of the column, while hot water feeds the top stage and flows toward the bottom. The amount of circulating water is adjusted to have the desired H_2O/CH_4 ratio in the wet biogas exiting the column (block #CL1 in Fig. 2). A saturation column has been preferred over steam mixing for humidification of biogas at relatively low pressure, as this reduces the demand of demi-water and it allows to recover the condensate from syngas cooling with no water treatment.

The wet biogas (#2) is preheated before feeding the eSMR reactor (#3), where it is converted into syngas (#4). The syngas exits the reformer at 7 bar and 800 °C and is cooled down in a heat exchanger (#HX2) where saturated steam at 8 bar is produced (#27). Syngas cooling by water evaporation prevents metal dusting of the tubes, which may occur with CO-rich streams and tube wall temperatures higher than 400–450 °C [24]. Syngas is cooled down to 300 °C (#5) and feeds the WGS reactor. The shifted syngas (#6) is cooled by preheating the wet biogas (#HX1) and then transfers heat to the bio-digester water loop (#HX3) and to the saturator make-up water (#HX4). Further cooling to 30 °C allows to separate the condensate, which is recovered and fed back into the saturator water loop (#21). Dry syngas (#11) is compressed to 30 bar and feeds the CO_2 separation section, where a methyl-diethanolamine (MDEA)-based solvent absorbs CO_2 in the absorption column (#CL2), then recovered at nearly atmospheric pressure from the top of the stripping column (#CL3). The CO_2 stream is delivered to the CO_2 compression and liquefaction unit, where liquid CO_2 (15 bar; −31 °C) is produced. Detailed information of the CO_2 liquefaction unit can be found in the supplementary material. The H_2-rich gas leaving the head of the absorption column (#13) feeds the PSA unit, where pure hydrogen is recovered (#14), while the PSA off-gases (#15), which contain unconverted CH_4, CO, CO_2 and unrecovered H_2, are burned in the boiler to produce saturated steam at 8 bar (#28). The steam generated by syngas cooling and off-gas combustion is used in the reboiler to regenerate the CO_2-rich solvent (#29), to heat up the water feeding the saturator (#30) and to heat up the water in the bio-digester circuit (#31). Consequently, the system is thermally self-sufficient, and the only energy input is the electricity required for the electrified reformer, compressors, pumps, and auxiliaries.

2.2. System integration with renewable energy and storages

Fig. 3 shows the block diagram of the complete system including the electrified biogas reforming plant (eBGR), the biogas, syngas and hydrogen storage tanks and the power supply system with battery storage. The compressed biogas (stream $\#bg_1(t)$ in Fig. 3) has a constant flow rate and can either feed the storage tank or the syngas generation unit. The amount of electricity absorbed by the syngas generation section ($E_{syn}(t)$), as well as the steam required to sustain the saturation column ($\#steam_4(t)$) and the steam available from syngas cooling ($\#steam_1(t)$) are proportional to the quantity of biogas fed to the system ($\#bg_2(t)$). When filling the biogas tank, the flow rate fed to the chemical island is reduced, thus the amount of steam required and generated, as well as the syngas produced ($\#syn_1(t)$) decreases.

Dry syngas ($\#syn_1(t)$) can feed the syngas storage tank or bypass it to feed the compressor. The electricity required for the gas separation unit ($\#E_{gs}(t)$), the steam required to regenerate the MDEA-based solvent in the CO_2 separation process ($steam_3(t)$), the steam generated in the boiler ($steam_2(t)$) as well as the produced hydrogen ($H_{2,1}(t)$ and liquefied CO_2 ($CO_2(t)$) are proportional to the flow rate of syngas fed to the gas separation section ($syn_2(t)$).

Renewable electricity is produced from PV panels and wind turbines. The generation profiles of renewable energy over time ($E_{wind}(t)$, $E_{PV}(t)$) are an input to the optimization algorithm, while the optimal capacity of PV and wind is calculated through capacity multipliers (S_{PV} and S_{Wind} respectively). The renewable power available at each instant t can be directed to the eBGR system ($\#E_{ren,2}(t)$), charge the battery ($\#b_1(t)$) or delivered to the grid ($grid_{out}(t)$). The renewable energy entering the eBGR system is partly directed to the syngas generation section ($E_{ren,3}(t)$) and partly to the gas separation section ($E_{ren,4}(t)$).

In the following sections, two operating modes are considered to describe the behavior of the chemical island.

- **Inflexible operation**: gas storage units are not installed, the biogas produced by the biodigester is constrained to feed the chemical plant, which therefore operates at constant load throughout the year. The intermittency of variable renewables is entirely managed by the battery storage system and by the exchanges with the electric grid.

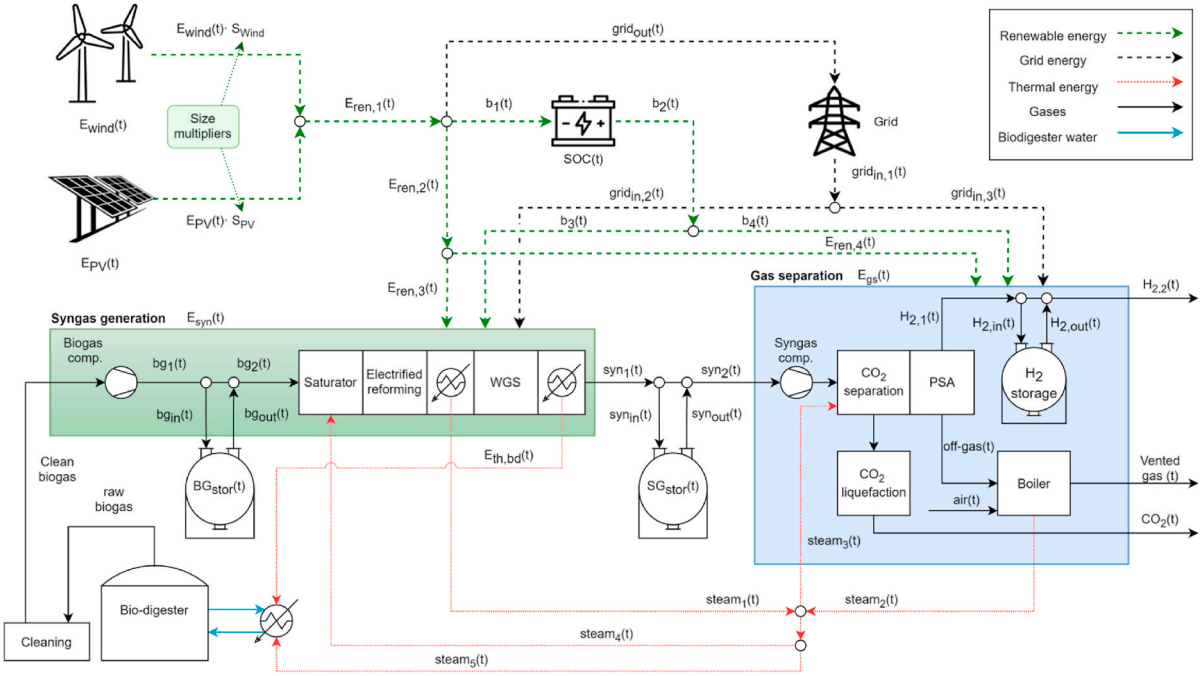

Fig. 3. Schematic of the integration of the eBGR system with power supply and storage systems and variables of the mathematical model.

- **Flexible operation**: gas storage units enable the two sections of the chemical island to vary the load independently. In this case, the intermittency of the variable renewables can also be managed by adapting the load of the plant sections.

3. Methods

3.1. Process simulation

The aforementioned eBGR system was modelled and simulated in Aspen Plus® by using the Peng-Robinson equation of state and the Electrolyte-NRTL for the amine-based absorption process, the saturation column and the water separation vessels. The saturation column is a packed column and is modelled with a rate-based approach. The circulating water is tuned to achieve a target H_2O/CH_4 ratio of 3.5 in the wet biogas, which was found to be the value that minimize the specific electric consumption per unit of produced hydrogen with the given reforming pressure and temperature (see the supplementary information for an analysis of the impact of the H_2O/CH_4 ratio on the plant performance). The eSMR and WGS reactors are modelled at chemical equilibrium. The eSMR reactor is assumed to be based on the technology developed by Ambrosetti et al. [10,12], using resistive heaters and copper-based thermally conductive internals to improve heat transfer in radial direction. Electric power is tuned to achieve a syngas outlet temperature of 800 °C, compatible with the copper internals. The WGS reactor is adiabatic. Both the absorption and stripping columns are tray columns, modelled with a rate-based approach [25]. Liquid-gas ratio in the absorber is tuned to separate 95% of the inlet CO_2. The stripper includes a condenser and a reboiler and is operated with a reflux and boil-up ratio resulting from the assumed temperatures of 70 °C and 120 °C [26,27]. The PSA unit works between 30 bar and is modelled as a simple separator with hydrogen recovery efficiency of 90% and off-gas outlet pressure of 1.4 bar.

The main assumptions for the process simulations are listed in Table 1.

3.2. Off-design simulation

The part-load operation of the chemical island is also evaluated with Aspen Plus®. Compressors and pumps isentropic and mechanical-electrical efficiency are assumed constant with flow-rate. Saturation column has a fixed geometry derived from plant simulation in design condition, as well as CO_2 absorption and stripper columns. The solvent flow rate in the absorber is varied to keep a constant CO_2 separation efficiency (95%). The power supply of the electrified reformer is controlled to keep a constant outlet temperature. Heat exchangers area is calculated at maximum load and heat transfer coefficients are varied depending on the fluids flow rate with an exponential law (Eq. (1), $n = 0.8$ for shell and tube and $n = 0.67$ for plate heat exchangers), while the overall heat transfer coefficient is calculated with Eq. (2), neglecting thermal resistance associated to the exchangers walls and fouling.

$$h_{off} = h_{design}\left(\frac{\dot{m}_{off}}{\dot{m}_{design}}\right)^{n}\left[\frac{W}{m^2K}\right] \quad (1)$$

$$U_{off} = \left(\frac{1}{h_{hot,off}} + \frac{1}{h_{cold,off}}\right)^{-1}\left[\frac{W}{m^2K}\right] \quad (2)$$

3.3. System optimization and integration

Integration with renewable sources, grid and storage units is modelled with GAMS optimization software and mixed integer linear programming (MILP) method. The functions linking the amount of gas fed to the chemical plant sections and the electricity absorbed, heat generated, and thermal load are derived from the partial load analysis of the chemical island.

Table 1
Summary of the process design and Aspen Plus® simulation assumptions.

Component	Parameter	Value	Unit
Saturation column (CL1)	Calculation mode: rate based, packed with pall ring		
	Target H_2O/CH_4 ratio	3.5	mol_{H2O}/mol_{CH4}
Electrified reformer (eSMR)	Calculation mode: chemical equilibrium		
	Outlet temperature	800	°C
	Inlet pressure	8	bar
	Pressure drop	1	bar
	Electric efficiency	99	%
WGS	Calculation mode: adiabatic, chemical equilibrium		
	Inlet temperature	300	°C
	Pressure drop	0.1	bar
Absorption column (CL2)	Calculation mode: rate-based with 10 stages		
	Pressure drop	0.3	bar
	CO_2 recovery efficiency	95	%
Stripping column (CL3)	Calculation mode: rate based, 10 stages plus partial vapor condenser and kettle reboiler		
	Condenser temperature	70	°C
	Condenser pressure	1.7	bar
	Lean ratio	0.015	mol_{CO2}/mol_{MDEA}
	Pressure drop	0.3	bar
Pressure Swing Adsorption (PSA)	H_2 recovery efficiency	90	%
	Pressure drop	1	bar
	Off-gas outlet pressure	1.4	bar
Pumps	Hydraulic efficiency	70	%
	Mechanical-electrical efficiency	94	%
Compressors	Volumetric with water cooling and outlet temperature of	120	°C
	Isentropic efficiency	70	%
	Mechanical-electrical efficiency	92	%
Pressure drops in heat exchangers	Gas side	2% p_{in}	%
	Water at 9 bar	0.9	bar
Heat transfer coefficients	Low pressure gas	50	$W/m^2/K$
	High pressure gas	500	$W/m^2/K$
	Biogas/Syngas in pre-heater	120[a]	$W/m^2/K$
	Syngas with condensing water	2500[a]	$W/m^2/K$
	Water (liquid)	10,000	$W/m^2/K$
	Water (evaporation)	20,000	$W/m^2/K$

[a] Values obtained with heat exchanger simulated in Aspen EDR (simulation mode) using inputs of streams from Aspen Plus.

The equations describing the behaviour of the plant are computed along the year with hourly resolution. Wind and solar power distribution is taken from Pfenninger et al. [28]. Energy balances between renewable power production, BESS, grid and electricity absorbed by the chemical plant are modelled through Equations (3)–(8).

$$E_{wind}(t) \bullet S_{wind} + E_{PV}(t) \bullet S_{PV} = E_{ren}(t) \quad (3)$$

$$E_{ren}(t) = E_{ren,2}(t) + b_1(t) + grid_{out}(t) \quad (4)$$

$$E_{ren,2}(t) = E_{ren,3}(t) + E_{ren,4}(t) \quad (5)$$

$$E_{syn}(bg_2(t)) = E_{ren,3}(t) + b_3(t) + grid_{in,2}(t) \quad (6)$$

$$E_{gs}(syn_2(t)) = E_{ren,4}(t) + b_4(t) + grid_{in,3}(t) \quad (7)$$

$$grid_{in,2}(t) + grid_{in,3}(t) = grid_{in}(t) \quad (8)$$

The BESS unit is charged when the renewable energy production is greater than the load and discharged when the renewable energy is not enough to sustain the eBGR system load. The battery is assumed to start and end the year completely discharged (Equation (9)) and is charged or discharged according to Equation (10), where η_c and η_d represent the charge and discharge efficiencies, respectively, and SOC(t) represents the state of charge. The charging and discharging efficiencies are equal

to 97%, a representative value of lithium-ion technology [29]. Battery capacity is an optimization variable (SOC_{max}) and consequently in each time period the state of charge has to be lower than the capacity, considering a depth of discharge of 80% (DoD in Eq. (11)). The Energy to Power ratio (EtP) is imposed equal to 4 h (Eq. (12)).

$$SOC(t=0)=0 \quad ; \quad SOC(t=8760)=0 \tag{9}$$

$$SOC(t)=SOC(t-1)+\left[b1(t)\eta_c-\frac{b2(t)}{\eta_d}\right]\Delta t \tag{10}$$

$$SOC(t) \le SOC_{max} \bullet DoD \tag{11}$$

$$b_1(t) \le SOC_{max}/EtP \; ; \; b_2(t) \le SOC_{max}/EtP \tag{12}$$

Equation (13) describes the mass balance at the gas storage boundaries, while Equation (14) is used to convert the mass flow rate to volumetric flow rate, with the gas density being a function of storage pressure and temperature. Storage tank volume is an optimization variable and is modelled using the same approach as for the BESS (Equations (15)–(17)).

$$bg_2(t)=bg_1(t)+bg_{out}(t)-bg_{in}(t) \tag{13}$$

$$\dot{V}_i(t)\left[m^3/h\right]=\dot{m}_i(t)\left[kg/h\right] \; / \; \left(\rho_i(p,T)\left[kg/m^3\right]\right) \tag{14}$$

$$BG_{stor}(t)=BG_{stor}(t-1)+\left[\dot{V}_{bg,in}(t)-\dot{V}_{bg,out}(t)\right]\Delta t \tag{15}$$

$$BG_{stor}(t) \le BG_{stor,max} \tag{16}$$

$$Stor(t=0)=0 \quad ; \quad Stor(t=8760)=0 \tag{17}$$

The energy balance of the steam generated within the chemical island is met with Equation (18). At each time step, the steam generated has to be greater than that required to regenerate the amines and sustain the saturator, as described by Equation (19).

$$steam_1(t)+steam_2(t)=steam_3(t)+steam_4(t)+steam_5(t) \tag{18}$$

$$steam_1(t)+steam_2(t) \ge steam_3(t)+steam_4(t) \tag{19}$$

3.4. Economic optimization

Table 2 presents the economic assumptions used for the chemical island, storages and renewable power generation. The economic analysis was carried out with the methodology of Turton [30] for the conventional components (pumps, heat exchangers, compressors, blowers and columns). The cost of each process unit is calculated taking into account the effect of pressure, construction material, direct and indirect project expenses, contingencies and contractor fees. The cost of the WGS and PSA units was taken from Ref. [31]. The electrified reformer cost was estimated with an in-house model estimating the amount of catalyst, electric resistances and internal thermally conductive structures [7]. The total reactor cost, including labour and installation costs, indirect costs, owner's and contingencies costs is obtained with the method from Riva et al. [32]. All costs are converted to € of year 2019 currency with the Chemical Engineering Plant Cost Index (CEPCI) [33]. Further details can be found in the supplementary material.

The biogas compressor, being located before the storage tank, works at constant load and is sized on the biogas flow rate produced by the biodigester. The eSMR reactor length was calculated to meet the constraints of maximum copper temperature (1000 °C) and pressure drops (1 bar), and is a function of the design space velocity (16 $Nm^3/h/kg_{cat}$) and catalyst loading (640 kg/m^3). Heat is supplied from the reactor core via electric wires [12], with assumed cost of 50 €/kW_{el}. The inner surface of the reactor is coated with a refractory (Insulfrax), with thickness determined to have 60 °C on the steel wall. The steel thickness is determined from the design pressure and material properties (316L steel

Table 2
Economic assumptions for renewable sources, storages and chemical island process units.

System integration	Short term	Long term	units	References
PV (fixed-tilt)				
Investment cost (Italy)	800	306	€/kW	[34,35]
Investment cost (Denmark)	1148	306	€/kW	
Fixed O&M costs	15	6	€/kW-y	
Variable O&M costs	0	0	€/kWh	
GWP emission	420–1400	420–1400	kg_{CO2eq}/kW	[36,37]
Wind (on-shore)				
Investment cost (Italy)	1500	1000	€/kW	[34,35]
Fixed O&M costs	45	20	€/kW-y	
Variable O&M costs	0	0	€/kWh	
GWP emission	380–650	380–650	kg_{CO2eq}/kW	[38]
Wind (off-shore)				
Investment cost (Denmark)	2449	2449	€/kW	[34,35]
Fixed O&M costs	101	80	€/kW-y	
Variable O&M costs	0	0	€/kWh	
BESS (lithium-ion)				
Charge efficiency	97%	97%	–	[34,35,39]
Discharge efficiency	97%	97%	–	
Energy/power ratio	4	4	kWh/kW	
Depth of Discharge (DoD)	80%	80%		
Investment cost	400	124	€/kWh	
Fixed O&M costs	10	2.5	€/kWh-y	
Variable O&M costs	0.13	0.04	€/MWh	
GWP emission	89–169	89–169	kg_{CO2eq}/kWh	[40]
Electrolyser				
Conversion efficiency EE to H_2 (LHV)	58.5%	68.0%	–	[35,41]
Investment cost	1300	363	€/kW	
Fixed O&M costs	26	12.7	€/kW-y	
Variable O&M costs	0.13	0.04	€/MWh	
H_2 storage				
charge efficiency	100%	100%	–	[42,43]
discharge efficiency	100%	100%	–	
Energy/power ratio	1752	1752	kWh/kW	
Investment Cost	10	0.49	€/kWh	
Fixed O&M costs	0.02	0.02	€/kWh-y	
Variable O&M costs	0	0	€/MWh	
Bio-Syngas storage				
charge efficiency	100%	100%	–	[44]
discharge efficiency	100%	100%	–	
Inv. Cost	62.3 [€/m^3] • V [m^3] + 66′223 [€]		€/m^3	
Fixed O&M costs	4% CAPEX			
Variable O&M costs	0	0		
Electricity purchased from grid	150	100	€/MWh	
Electricity delivered to the grid	0	0	€/MWh	
Grid electricity GWP emission	400	400	g_{CO2eq}/kWh	
Chemical Island				
eSMR reactor	346 [€/Nm^3] • V_{in} [Nm^3] + 13′260 [€]			In-house & [12,32]
Cooling water	$1.57 \bullet 10^{-5}$		€/kg	
Process water	$1.71 \bullet 10^{-3}$		€/kg	
Catalyst replacement, every 5 year (Rhodium)	2000		€/kg	
Fixed O&M costs	4% CAPEX			
Other process equipment	Detail in supplementary material			[45]
Heat for biodigester	15% of biogas LHV power			

with design stress at 300 °C) [32,46]. The eSMR reactor is designed to process the maximum flow rate of biogas, and its cost function is linear with respect to inlet flow (see supplementary material).

The maximum capacity is an optimization variable and represents the maximum flow rate of biogas and syngas feeding the syngas generation and gas separation units, respectively ($bg_2(t)$ and $syn_2(t)$ flows in Fig. 3), while the hydrogen flow rate exiting the storage is constant (flow $H_{2,2}(t)$ in Fig. 3). Equation (20) represents the constraint on the biogas and syngas flow rates. As the biogas or syngas maximum flow rate increases, the CAPEX of the syngas generation (excluding the eSMR reactor) and gas separation section varies with exponential scaling law as shown in Equation (21) [47], where the reference costs are those presented in Fig. 5 and refer to the flow rate of biogas produced by the biodigester, and the exponential coefficient n is equal to 0.66.

$$\mathrm{BG}_2(t) \le capacity_{max,BG};\ \mathrm{Syn}_2(t) \le capacity_{max,Syn} \tag{20}$$

$$CAPEX_i = CAPEX_{ref,i}\left(\frac{Capacity_{max,i}}{Capacity_{ref,i}}\right)^n \tag{21}$$

The objective function is the total annual costs, which is minimized using the CPLEX solver.

$$\textbf{Objective function}: Min\ (Cost)$$
$$Cost = CAPEX \bullet CCF + fOPEX + vOPEX \tag{22}$$

The carrying charge factor (CCF) is assumed to be 10%, which corresponds to a discount rate of 8% over 25 years lifetime.

The optimization variables are the capacity of renewable plants, of BESS and of gas storage units. Nonlinear economic equations coupling gas flow rate with plant cost (Eq. (21)) allow the calculation of the optimal size of chemical island equipment and were linearized with the piecewise method [48].

3.5. Emissions

To estimate the climate impact of the process, equivalent CO_2 emissions are computed including the embedded emissions in PV, wind and BESS units. For PV panels, values between 420 $kg_{CO2,eq}/kW_{el}$ for a glass-glass single-Si produced in EU [36] and 1400 $kg_{CO2,eq}/kW_{el}$ for a single-Si panel produced in China [37] have been considered. GWP emission of wind turbines is derived from the work of Schreiber et al., who reported values between 380 and 650 $kg_{CO2,eq}/kW_{el}$ depending on the size of the turbine and amount of electricity used for production [38]. Embedded emission of Li-Ion battery varies between 89 and 169 $kg_{CO2,eq}/kWh_{el}$ depending on the lithium source, manufacturing scenario, and the bill of materials [40,49]. For imported grid electricity, emissions are assumed to be 400 kg_{CO2}/MWh, consistent with power generation from a natural gas combined cycle.

3.6. Key performance indicators

The Hydrogen production ratio (HR) measures the LHV power contained in the hydrogen produced with respect to the LHV power in the biogas feedstock (Eq. (23))

$$HR = \frac{\dot{m}_{H2} \bullet LHV_{H2}}{\dot{m}_{BG} \bullet LHV_{BG}}\ \left[\frac{kW_{H2}}{kW_{gas}}\right] \tag{23}$$

The specific CO_2 emissions ($E_{CO2,emit}$) and specific captured CO_2 ($E_{CO2,capt}$) compute the amount of carbon dioxide emitted and captured in relation to the produced hydrogen (Eqs. (24) and (25))

$$E_{CO2,emit} = \frac{\dot{m}_{CO2,emit}}{\dot{m}_{H2}}\ \left[\frac{kg_{CO2}}{kg_{H2}}\right] \tag{24}$$

$$E_{CO2,capt} = \frac{\dot{m}_{CO2,capt}}{\dot{m}_{H2}}\ \left[\frac{kg_{CO2}}{kg_{H2}}\right] \tag{25}$$

The carbon capture ratio (CCR) represents the molar ratio between the liquefied CO_2 and the inlet carbon from biogas (Eq. (26)).

$$CCR = \frac{\dot{n}_{CO2,liquefied}}{\dot{n}_{C,inlet}} \tag{26}$$

The specific electricity consumption (E_{el}) represents the net electricity consumed by the system per unit of hydrogen produced (Eq. (27))

$$E_{el} = \frac{P_{el}}{\dot{m}_{H2}}\ \left[\frac{kWh_{el}}{kg_{H2}}\right] \tag{27}$$

The renewable energy share (RENS) represents the share of renewable electricity used by the plant during the year with respect to the total electric energy consumed (Eq. (28)).

$$RENS = \frac{\sum_{t=1}^{8760}\left(E_{ren,2}(t) + b_2(t)\right) \bullet \Delta t}{\sum_{t=1}^{8760}\left(E_{syn}(t) + E_{gs}(t)\right) \bullet \Delta t} \bullet 100\ [\%] \tag{28}$$

The battery equivalent cycle number (BCY) represents the ratio of renewable energy fed to the battery and its capacity (Eq. (29)). This parameter provides an estimate of the number of charge/discharge cycles performed by the battery during the year.

$$BCY = \frac{\sum_{t=1}^{8760} b_1(t) \bullet \Delta t}{SOC_{max}}\ \left[\frac{kWh}{kWh}\right] \tag{29}$$

The capacity of the biogas, syngas and hydrogen storage vessels is expressed in terms of storage hours (STH) and calculated as the ratio between the storage tank volume and the maximum volumetric flow rate of gas fed (Eq. (30)). Thus, it corresponds to the hours required to fill or empty the tank at maximum flow rate.

$$STH = \frac{BG_{stor,max}}{\dot{V}_{bg1}}\ [h] \tag{30}$$

The levelized cost of electricity (LCOE) of PV and Wind is calculated taking into account the amortised investment cost and the annual operation and maintenance costs, considering the annual energy produced by the corresponding plants (Eq. (31)). The cost of renewable used energy ($LCOE_u$) by the chemical island is calculated neglecting the excess electricity, which is considered as curtailed (Eq. (32)).

$$LCOE_{PV\ or\ Wind} = \frac{(CAPEX_{PV\ or\ Wind}) \bullet CCF + fixed\ O\&M + var\ O\&M}{EE_{PV\ or\ Wind}}\ \left[\frac{€}{MWh}\right] \tag{31}$$

$$LCOE_u = \frac{CAPEX_{PV+wind+BESS} \bullet CCF + \sum fixed\ O\&M + \sum var\ O\&M}{\sum_{t=1}^{8760}\left(E_{ren,2}(t) + b_2(t)\right)}\ \left[\frac{€}{MWh}\right] \tag{32}$$

4. Results

4.1. Biogas to hydrogen plant

The KPIs of the simulated biogas to hydrogen plant are reported in Table 3. The plant achieves over 95% of CH_4 conversion in the reformer, and 73% CO conversion in the WGS, leading to about 70% of total CH_4 conversion to CO_2. Overall, the plant achieves a carbon capture ratio of 75.9%, leading to specific biogenic CO_2 emissions of 3 kg_{CO2}/kg_{H2} and specific CO_2 capture rate of 9.4 kg_{CO2}/kg_{H2}. Almost all the chemical energy of the biogas is retained in the hydrogen product, as the H_2

Table 3
Main results and KPIs of the biogas to hydrogen plant at mean load.

		eBGR system
CH_4 conversion in eSMR	%	95.1%
CO conversion in WGS	%	73.2%
Electricity consumption breakdown		
Blowers, pumps and coolers	kW_{el}	21.6
Biogas compressor	kW_{el}	50.9
Syngas compressor	kW_{el}	96.0
eSMR	kW_{el}	850.1
CO_2 compressors	kW_{el}	77.2
Total	kW_{el}	1095.8
Biogas thermal input	kW_{LHV}	2142
Hydrogen thermal output	kW_{LHV}	2064
CO_2 specific emission	kg_{CO2}/kg_{H2}	3.00
Specific captured CO_2	kg_{CO2}/kg_{H2}	9.42
Carbon capture ratio	%	75.94
H_2 production ratio	MW_{H2}/MW_{BG}	96.34%
Specific electricity consumption	kWh_{el}/kg_{H2}	17.69

production ratio is equal to 96%. The specific electricity consumption is 17.7 kWh/kg_{H2}, of which 78% for the electrified reformer, followed by the compression of syngas (9%), CO_2 (7%) and biogas (5%), respectively.

Fig. 4 shows the T-Q diagrams related to syngas cooling and exploitation of the steam generated by the plant, under design (Fig. 4a and b) and partial load (Fig. 4c and d) conditions. In all the operating conditions, the heat required to sustain the system, including the heating of the biodigester, is recovered from the process.

The breakdown of CAPEX of the eBGR system is shown in Fig. 5. The total capital expenditure is equal to 3.47 M€ (i.e. 1684 €/kW_{H2}). The cost associated with the separation of CO_2 from syngas and its further compression and liquefaction represents the largest contribution on the investment, amounting to 1.4 M€. The cost associated with the compression of biogas and syngas is equal to 0.56 M€ and the investment for the electrified reformer amounts to 0.41 M€. In the flexible system, oversized to be fed with 150% of the flow rate compared to design conditions, CAPEX increases to 5.0 M€ (i.e. 2440 €/kW_{H2}, referred to the average H_2

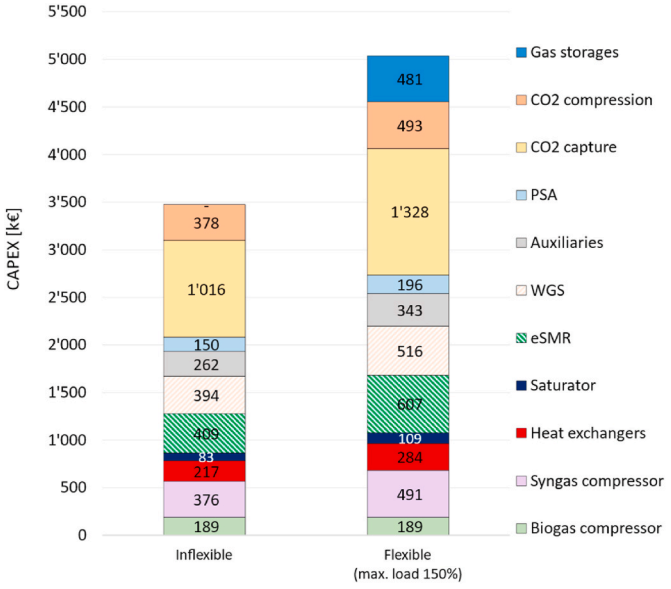

Fig. 5. Capital expenditure breakdown for the inflexible and flexible (maximum eSMR load = 150% of the average load) plants.

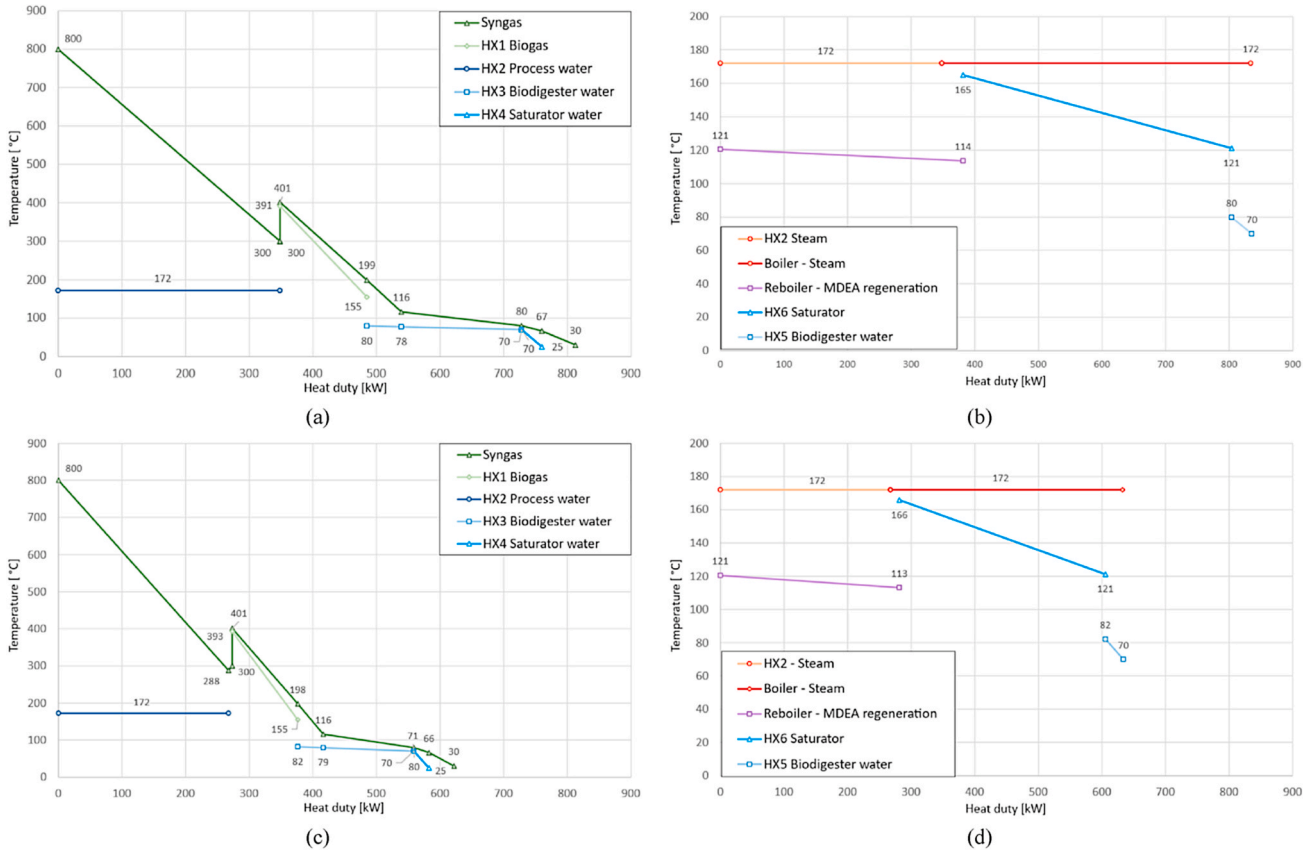

Fig. 4. TQ diagram of the syngas cooling line (a) and steam (b) in design and part load condition with a 25% reduction in biogas flow (c), (d). Heat exchangers codes in the legend refer to the notation in Fig. 2.

Table 4
LCOE and Capacity factor of PV and Wind for the selected locations in short-term and long-term scenarios.

Location	unit	North Italy	South Italy	Denmark
WIND				
Capacity Factor	%	14.9%	27.3%	55.1%
LCOE Wind, short-term	€/MWh	149.1	81.7	71.7
LCOE Wind, long-term	€/MWh	91.8	50.3	71.7
PV				
Capacity Factor	%	16.9%	18.9%	9.9%
LCOE PV, short-term	€/MWh	64.3	57.2	149.9
LCOE PV, long-term	€/MWh	24.8	22.0	42.3

production capacity) and gaseous storage tanks account for 0.48 M€.

4.2. System integration and economic optimization

The integration of the biogas to hydrogen plant with renewable energy sources is assessed for three locations: (i) Piemonte, in North Italy, one of the European regions with the highest biogas production capacity, featuring good availability of solar energy and low availability of wind energy; (ii) Sicily, in South Italy, representative of a region with high availability of solar energy and average availability of wind energy and (iii) Denmark, another European region with large biogas production capacity, featuring very high wind energy availability and low solar energy availability. Table 4 shows the capacity factor (CF) and the LCOE

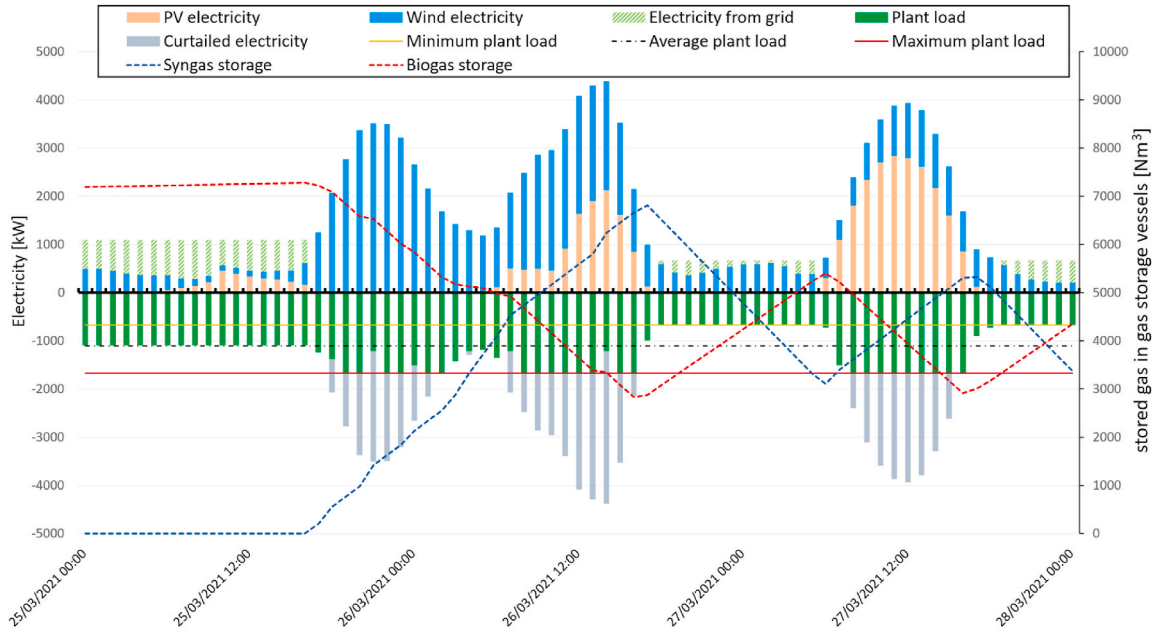

(a) Flexible system

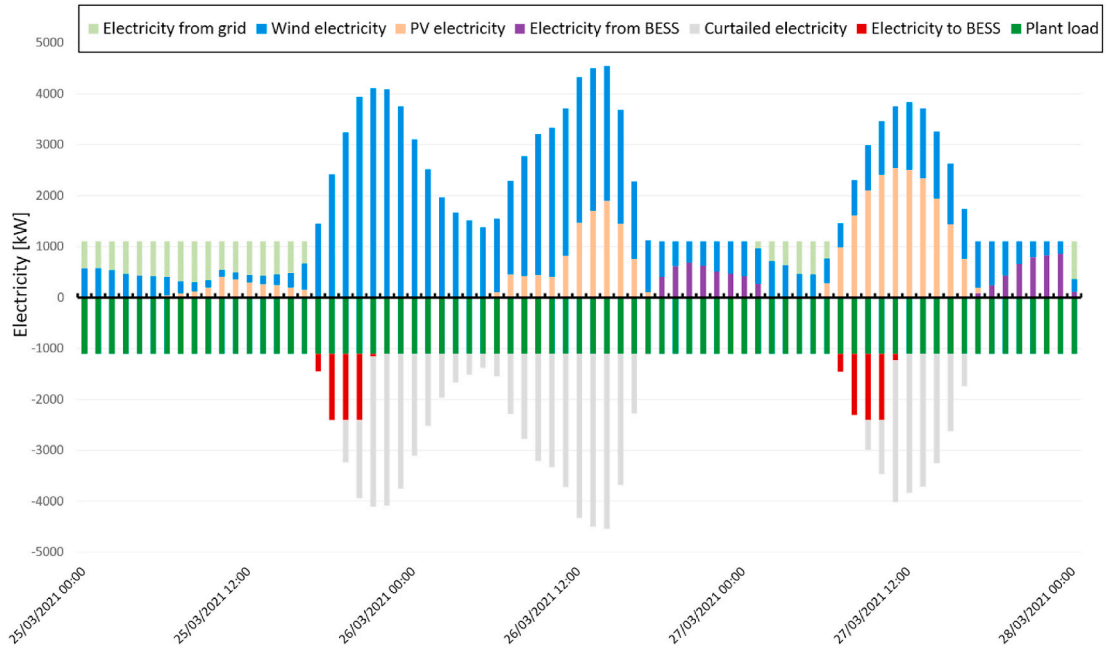

(b) Inflexible system

Fig. 6. Hourly energy balance of (a) flexible system and (b) inflexible system in North Italy at RENS = 80% in three representative spring days.

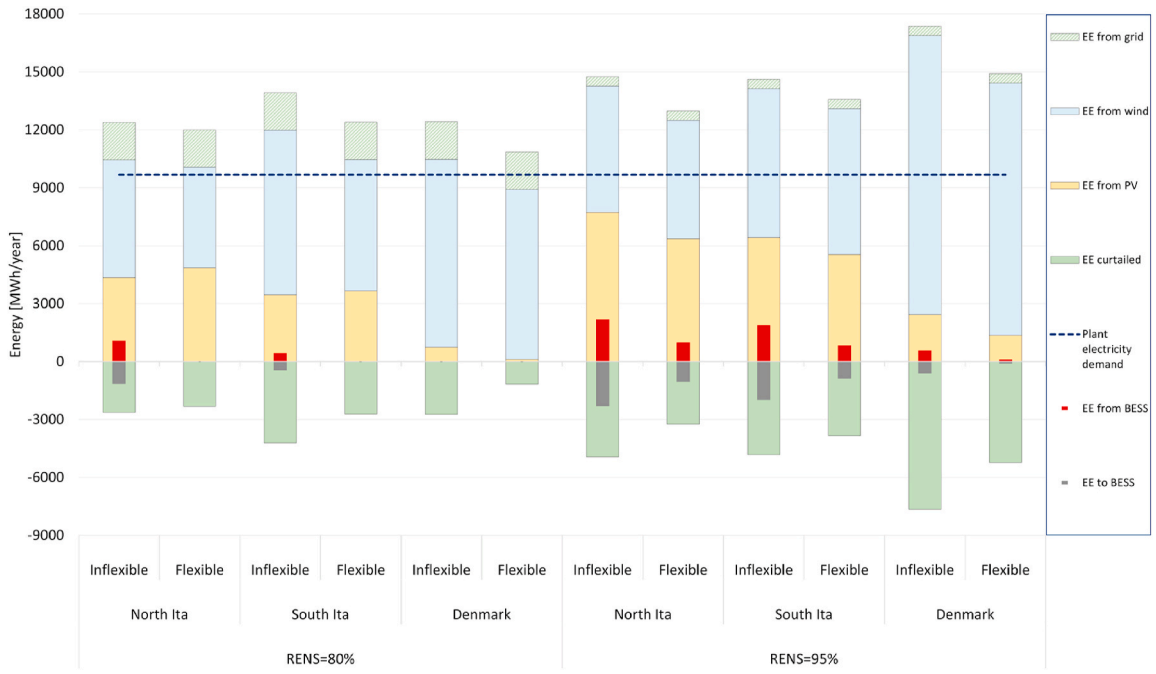

Fig. 7. Annual energy balance breakdown for inflexible and flexible systems, with RENS = 80% and 95%, in the short-term cost scenario.

of PV and wind electricity produced in these regions in the short- and long-term cost scenarios.

4.2.1. *Energy balance and renewable capacity*

To illustrate the operation of the yearly simulation model, Fig. 6a shows the hourly energy balance over three representative days of the flexible system in North Italy with renewable energy share (RENS) of 80%, optimized in the short-term cost scenario (hourly profiles of the other scenarios are available in the supplementary information). This optimized plant does not include battery storage and hydrogen storage vessel. The positive columns represent electricity inputs and the negative columns represent the electricity consumed by the process and the curtailed electricity. The dotted lines (referred to the secondary axis) represent the state of charge of the gas storage tanks. In the first hours of

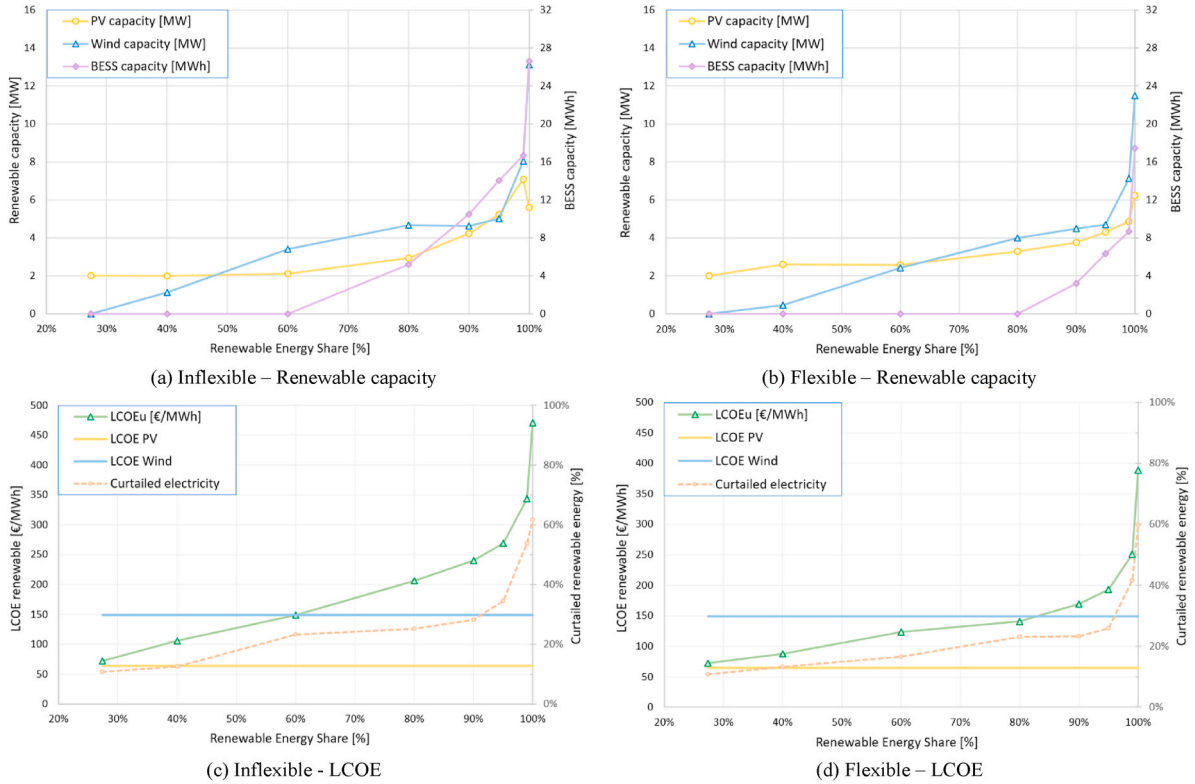

Fig. 8. Installed capacity of PV, Wind and BESS in the Inflexible (a) and Flexible (b) cases in north Italy as a function of RENS; LCOE of renewable energy in Inflexible (c) and Flexible (d) cases in North Italy as a function of RENS, in the short-term cost scenario.

Table 5
Main results of the optimized plants at 95% RENS in different scenarios.

Location		North Ita							
Plant size		Small-scale				Large-scale			
Cost-scenario		short-term		long-term		short-term		long-term	
Flexibility		No	Yes	No	Yes	No	Yes	No	Yes
Biogas input	Nm^3/h	391	391	391	391	3915	3915	3915	3915
Biogas thermal Input	MW_{LHV}	2.14	2.14	2.14	2.14	21.42	21.42	21.42	21.42
PV capacity	MW	5.23	4.30	7.39	6.10	52.40	43.28	73.95	61.04
Wind capacity	MW	5.01	4.70	2.71	2.63	49.98	45.49	27.10	27.44
BESS capacity	MWh	14.05	6.35	18.94	13.35	140.54	63.27	189.40	119.27
BESS eq. cycles	–	165	164	180	196	165	164	180	197
Biogas storage	m^3	–	1367	–	1150	–	14,137	–	12,044
Biogas storage hours	h	–	28	–	23	–	29	–	24
Syngas storage	m^3	–	3370	–	2040	–	29,411	–	12,507
Syngas storage hours	h	–	17	–	10	–	15	–	6
Hydrogen storage	m^3	–	188	–	254	–	2751	–	4318
Hydrogen storage hours	h	–	7	–	9	–	10	–	15
Syngas generation relative size	%	100%	159%	100%	134%	100%	167%	100%	142%
CO_2 separation relative size	%	100%	138%	100%	105%	100%	149%	100%	115%
H_2 output	Nm^3/h	688	688	688	688	6887	6887	6887	6887
H_2 thermal output	MW_{LHV}	2.06	2.06	2.06	2.06	20.63	20.63	20.63	20.63
CO_2 captured	t/y	5114	5114	5114	5114	51,139	51,139	51,139	51,139
$LCOE_{ren}$	€/MWh	269	193	110	92	269	190	110	90
EE curtailed	%	35%	26%	35%	25%	35%	25%	35%	26%
H_2 production cost	€/kg	7.11	6.25	7.11	6.25	5.88	4.86	3.14	2.95
REN $CO_{2,eq}$emissions (low-/high-emission scenarios)	kg_{CO2}/kg_{H2}	0.46/1.13	0.35/0.88	0.52/1.38	0.42/1.12	0.46/1.13	0.35/0.88	0.52/1.38	0.42/1.12
Grid emissions	kg_{CO2}/kg_{H2}	0.36	0.36	0.36	0.36	0.36	0.36	0.36	0.36
CO_2 capture	kg_{CO2}/kg_{H2}	−9.42	−9.42	−9.42	−9.42	−9.42	−9.42	−9.42	−9.42
Net emissions (low-/high-emission scenarios)	kg_{CO2}/kg_{H2}	−8.61/−7.93	−8.72/−8.19	−8.55/−7.69	−8.65/−7.95	−8.61/−7.93	−8.72/−8.19	−8.55/−7.69	−8.66/−7.96
Location		South Ita							
Plant size		Small-scale				Large-scale			
Cost-scenario		short-term		long-term		short-term		long-term	
Flexibility		No	Yes	No	Yes	No	Yes	No	Yes
Biogas input	Nm^3/h	391	391	391	391	3915	3915	3915	3915
Biogas thermal Input	MW_{LHV}	2.14	2.14	2.14	2.14	21.42	21.42	21.42	21.42
PV capacity	MW	3.87	3.34	4.92	4.71	38.66	35.40	49.23	45.64
Wind capacity	MW	3.23	3.16	1.52	1.74	32.33	29.33	15.15	17.33
BESS capacity	MWh	11.74	5.17	15.27	9.80	117.43	50.05	152.70	85.73
BESS eq. cycles	–	169	168	216	214	169	160	216	214
Biogas storage	m^3	–	1500	–	607	–	13,096	–	12,230
Biogas storage hours	h	–	30	–	12	–	26	–	25
Syngas storage	m^3	–	3374	–	1393	–	29,720	–	8628
Syngas storage hours	h	–	17	–	7	–	15	–	4
Hydrogen storage	m^3	–	239	–	93	–	1815	–	4532
Hydrogen storage hours	h	–	8	–	3	–	6	–	16
Syngas generation relative size	%	100%	144%	100%	133%	100%	160%	100%	147%
CO_2 separation relative size	%	100%	117%	100%	102%	100%	140%	100%	122%
H_2 output	Nm^3/h	688	688	688	688	6887	6887	6887	6887
H_2 thermal output	MW_{LHV}	2.06	2.06	2.06	2.06	20.63	20.63	20.63	20.63
CO_2 captured	t/y	5114	5114	5114	5114	51,139	51,139	51,139	51,139
$LCOE_{ren}$	€/MWh	200	142	78	66	200	137	78	63
EE curtailed	%	34%	29%	20%	22%	34%	28%	20%	21%
H_2 production cost	€/kg	5.95	5.28	3.84	3.80	4.71	3.93	2.60	2.49
REN $CO_{2,eq}$emission (low-/high-emission scenarios)	kg_{CO2}/kg_{H2}	0.34/0.84	0.26/0.66	0.36/0.95	0.31/0.84	0.36/0.82	0.26/0.68	0.36/0.95	0.29/0.79
Grid emissions	kg_{CO2}/kg_{H2}	0.36	0.36	0.36	0.36	0.36	0.36	0.36	0.36
CO_2 capture	kg_{CO2}/kg_{H2}	−9.42	−9.42	−9.42	−9.42	−9.42	−9.42	−9.42	−9.42
Net emission (low-/high-emission scenarios)	kg_{CO2}/kg_{H2}	−8.73/−8.23	−8.81/−8.4	−8.71/−8.12	−8.76/−8.22	−8.71/−8.25	−8.81/−8.39	−8.71/−8.12	−8.78/−8.28

Location		Denmark							
Plant size		Small-scale				Large-scale			
Cost-scenario		short-term		long-term		short-term		long-term	
Flexibility		No	Yes	No	Yes	No	Yes	No	Yes
Biogas input	Nm^3/h	391	391	391	391	3915	3915	3915	3915
Biogas thermal Input	MW_{LHV}	2.14	2.14	2.14	2.14	21.42	21.42	21.42	21.42
PV capacity	MW	2.80	1.56	6.51	4.79	27.99	15.89	65.06	45.78
Wind capacity	MW	2.99	2.71	1.55	1.52	29.95	26.83	15.46	15.51
BESS capacity	MWh	8.41	1.35	14.55	7.40	84.11	14.00	145.51	67.82
BESS eq. cycles	–	72	73	98	97	72	73	98	86
Biogas storage	m^3	–	1781	–	1507	–	17,869	–	15,074
Biogas storage hours	h	–	36	–	30	–	36	–	30
Syngas storage	m^3	–	5555	–	2729	–	52,765	–	16,692
Syngas storage hours	h	–	28	–	14	–	26	–	8
Hydrogen storage	m^3	–	–	–	93	–	788	–	5260
Hydrogen storage hours	h	–	0	–	3	–	3	–	18
Syngas generation relative size	%	100%	133%	100%	128%	100%	133%	100%	135%
CO_2 separation relative size	%	100%	102%	100%	103%	100%	103%	100%	113%
H_2 output	Nm^3/h	688	688	688	688	6887	6887	6887	6887
H_2 thermal output	MW_{LHV}	2.06	2.06	2.06	2.06	20.63	20.63	20.63	20.63
CO_2 captured	t/y	5114	5114	5114	5114	51,139	51,139	51,139	51,139
$LCOE_{ren}$	€/MWh	206	133	114	91	206	132	110	87
EE curtailed	%	45%	36%	29%	20%	45%	36%	29%	19%
H_2 production cost	€/kg	6.05	5.06	4.43	4.25	4.81	3.76	3.14	2.89
REN $CO_{2,eq}$ emissions (low-/high-emission scenarios)	kg_{CO2}/kg_{H2}	0.26/0.64	0.15/0.35	0.41/1.14	0.29/0.81	0.26/0.64	0.15/0.36	0.41/1.14	0.28/0.77
Grid emissions	kg_{CO2}/kg_{H2}	0.36	0.36	0.36	0.36	0.36	0.36	0.36	0.36
CO_2 capture	kg_{CO2}/kg_{H2}	−9.42	−9.42	−9.42	−9.42	−9.42	−9.42	−9.42	−9.42
Net emissions (low-/high-emission scenarios)	kg_{CO2}/kg_{H2}	−8.81/−8.43	−8.92/−8.72	−8.65/−7.93	−8.78/−8.26	−8.81/−8.43	−8.92/−8.71	−8.65/−7.93	−8.79/−8.3

the considered time frame, the biogas storage tank is full, the syngas storage tank is empty and the plant operates at its average load, i.e. converting all the incoming biogas with no gas flows into or from the storage vessels. In this time period, the renewable energy production is low and part of the electricity is purchased from the grid. When renewable production increases, the biogas storage empties, enabling an increase of syngas production and of electricity consumption up to the maximum plant load. At the same time, the syngas storage tank charges. In some hours, renewable production is greater than the plant load and excess electricity is curtailed. When renewable production drops again (evening of March 26th), the plant starts operating at its minimum load, minimizing electricity consumption and requiring biogas storage charging and syngas storage discharging. Subsequently, when renewable production returns (day of March 27th), the biogas tank empties and the load of the plant increases again to its maximum load. Fig. 6b shows the hourly energy balance over the same period of the inflexible system with the same RENS. Renewable variability can only be managed by the battery and by electricity absorption from the electric grid, which leads to an increase in renewable capacity and higher curtailment.

Fig. 7 shows the annual energy balance for different locations and different RENS for the optimized inflexible and flexible systems with the short-term cost scenario. The positive columns represent energy inputs from the grid, PV and wind, while the negative columns represent excess curtailed electricity. Additionally, Fig. 7 depicts the fraction of renewable energy that is conveyed to and withdrawn from the BESS. At the same renewable energy share, the flexible plant allows for better utilisation of renewable production peaks, reducing the curtailment and the need of BESS. In the Italian locations, the share of PV and wind are comparable. In all the Danish cases, electricity generation is dominated by wind power and lower BESS size is required, thanks to the more stable profile of wind power generation.

Fig. 8a and c show the optimal capacity of PV, wind and BESS, and the corresponding $LCOE_u$ as function of RENS for inflexible and flexible plant in North Italy in the short-term cost scenario. The $LCOE_u$ is comprised between the LCOE of PV and wind technologies as long as the BESS system is not installed and as long as the curtailed energy is small. In the flexible case (Fig. 8b and d), the reduced capacity of renewables and BESS lead to reduced curtailed energy and lower $LCOE_u$.

When the system is constrained not to use electricity from the grid (i.e., RENS = 100 %), the renewable and battery capacity, the curtailed electricity and the $LCOE_u$ grow abruptly.

Table 5 provides the optimal size of syngas generation and gas separation. The maximum size of syngas generation island is achieved for RENS between 80 and 95 % and is 133–165 % of the size of the inflexible system processing the given biodigester flow rate. The capacity of the gas separation section is always lower than the syngas generation section, being the most capital intensive section of the plant. Consequently, it is preferable to increase the volume of the syngas tank rather than oversize this section of the plant.

4.2.2. *Economic analysis*

Fig. 9a depicts the CAPEX breakdown of the assessed systems in the short-term cost scenario, including the breakdown of the biogas to hydrogen plant into the two sections of syngas generation and gas separation. Most of the total system capital costs are associated to the cost for renewable power generation. The CAPEX of the biogas to hydrogen plant (including the gas storage units) ranges from 17% in the RENS-95% North Italy inflexible case to 47% in the RENS-80% Denmark flexible case, in the short-term scenario. In the long-term scenario, due to the reduced cost of renewables, the CAPEX share of the chemical plant increases to 31–55%. The flexibility of the system leads to a reduction in the total investment costs, as the increased cost associated with the installation of the storage tanks and the increased size of the chemical island equipment is more than offset by the reduced investment cost of renewables and battery capacities. In the case with RENS = 95%, the cost reduction obtained with the flexible plant is the greatest, mainly

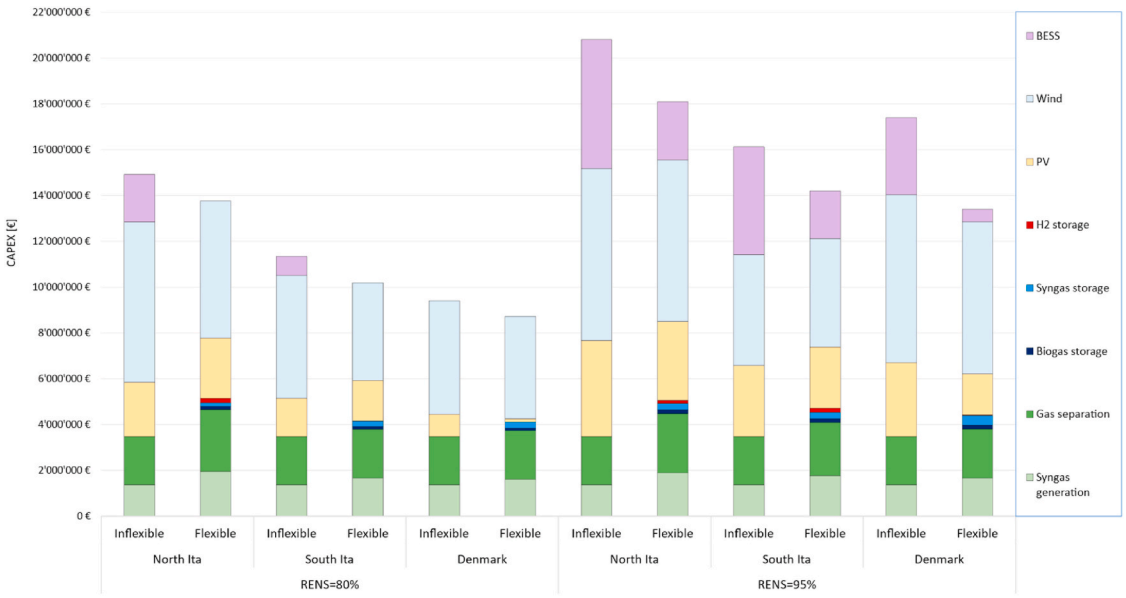

(a) Short-term scenario

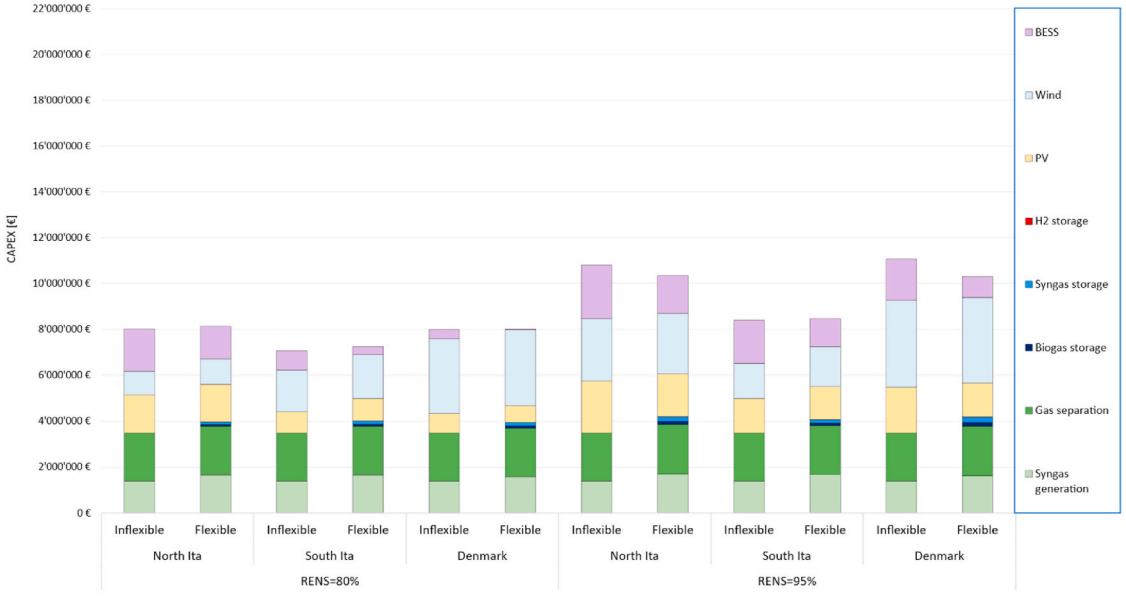

(b) Long-term scenario

Fig. 9. CAPEX breakdown for inflexible and flexible system in different locations for the short-term (a) and long-term (b) cost scenario.

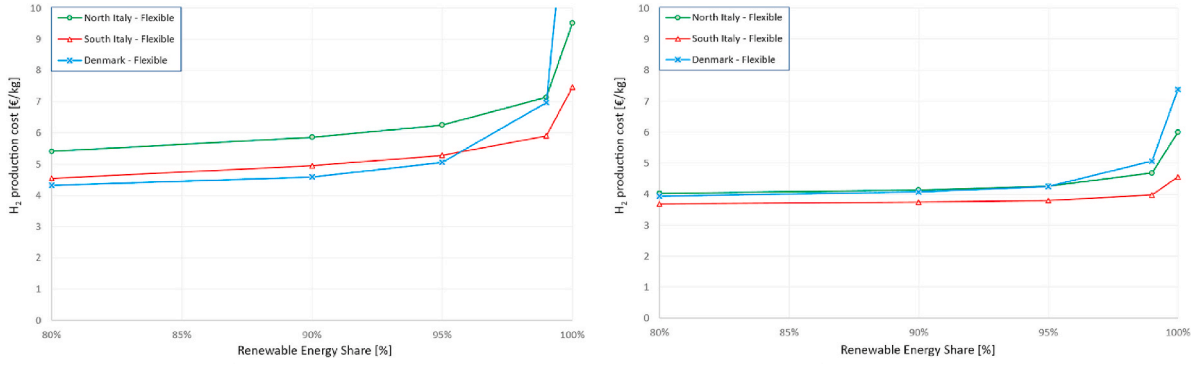

(a) Short-term scenario (b) Long-term scenario

Fig. 10. H_2 production cost as a function of RENS for short-term (a) and long-term (b) cost scenarios with flexible plants.

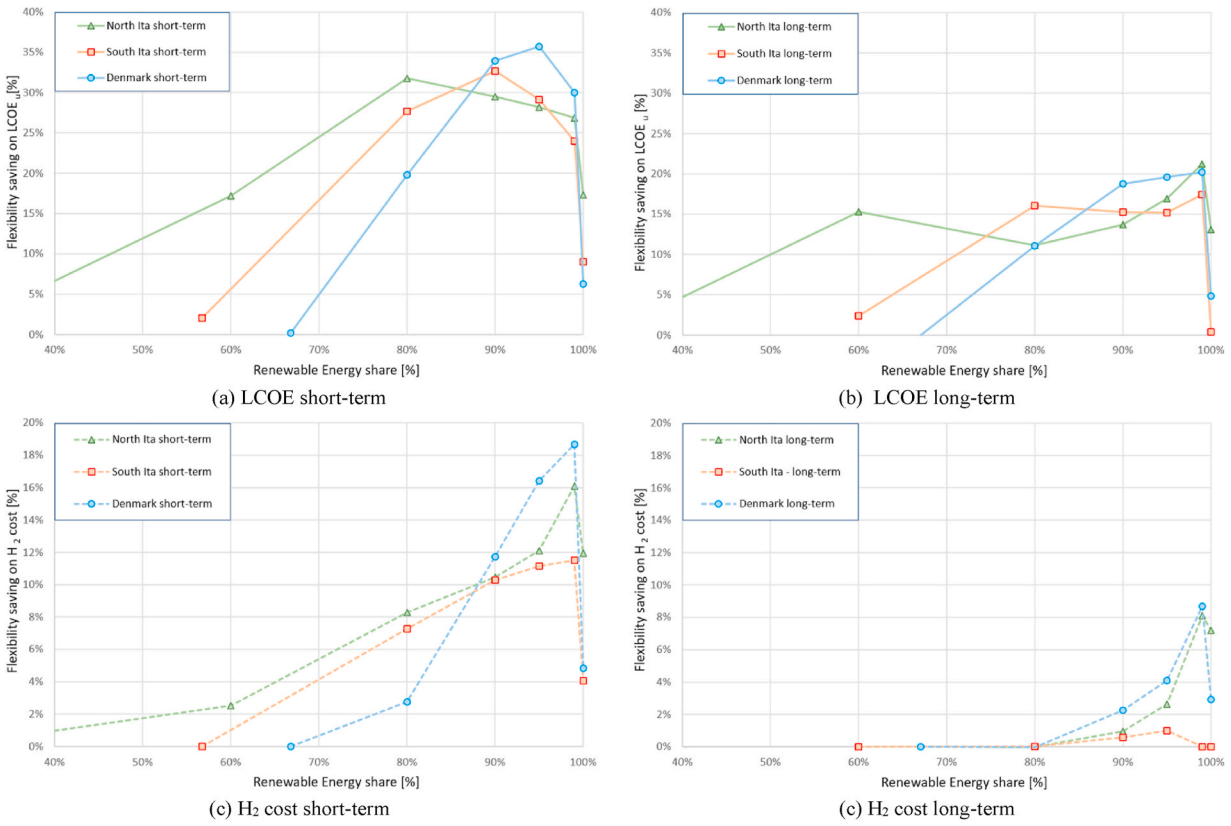

Fig. 11. Flexibility-related savings on LCOE (a) and hydrogen production cost (b) in the short-term scenario.

because the high battery capacity required in the inflexible plant. The flexible Danish case results in the lowest CAPEX. In contrast, the North Italy case is the most expensive, as a result of the lower capacity factor of renewables. In the long-term scenario (Fig. 9b), the reduced costs of renewables and batteries lead to a diminished benefit from system flexibility. For instance, in South Italy, the CAPEX of the flexible system is slightly higher, due to the increased costs associated with the chemical island and storages, which do not fully compensate for the reduced costs of renewables and battery storage.

As depicted in Fig. 10a for the short-term scenario and Fig. 10b for the long-term scenario, the investment costs and the hydrogen cost increase as RENS rises, as a result of the higher capacity of renewables and battery installed. It can be noted that the increase in production cost is relatively small up to RENS = 95%. To achieve an off-grid operation (i.e. 100% RENS), the hydrogen production cost increases significantly. In the short-term scenario, the hydrogen production cost is between 4.3 and 5.4 €/kg when the renewable share is 80 %. Costs are lower and similar in the Denmark and South Italy cases and higher in the North Italy case. Increasing the RENS to 95% leads to an increase of the production cost up to 5.1–6.2 €/kg. At 100% RENS, the cost increases abruptly to 7.5–9.5 €/kg in Italian cases and to over 10 €/kg in the Danish case.

In the long-term scenario, the lower cost of renewable sources and battery leads to reduced cost increase with the renewable share, as well as lower cost of hydrogen. In the case with RENS = 80%, the cost of hydrogen is between 3.7 and 4.0 €/kg and increases up to 3.8–4.3 €/kg with RENS = 95% and to 4.6–7.4 €/kg with RENS = 100%.

The savings on $LCOE_u$ achievable with the flexible plant compared to the inflexible plant is depicted in Fig. 11a for the short-term economic scenario. As the share of renewables increases, the benefit increases to a maximum of up to 30–35% and then decreases to 5–20% in the 100% RENS case due to the significant oversizing of renewables and battery capacity. As depicted in Fig. 11c for the short-term scenario, the savings on the cost of hydrogen production is lower, as the reduced renewable energy cost is partly balanced by the higher plant cost and, more importantly, as a major fraction of the hydrogen cost is associated to biogas cost, which is unaffected by the plant flexibility. In any case, flexibility allows the hydrogen cost to be reduced by up to about 10–12% in Italy and up to 18% in Denmark, above 90% RENS. In the long-term scenario (Fig. 11b) the flexibility-related saving on $LCOE_u$ is still maximum above 90% RENS but reduced and equal to 15–20%. The maximum benefit on hydrogen production cost is reduced and equal to 1–9%.

Fig. 12a depicts the breakdown of the hydrogen production cost in the short and long-term scenario with RENS = 95%. As shown in Fig. 12a, the cost of biogas is the most impactful item for the cost of hydrogen, accounting for 1.9 €/kg with the assumed biogas cost of 55 €/MWh. The CAPEX of the chemical island accounts from 0.64 €/kg in inflexible systems to 0.83 €/kg in flexible plants. In flexible plants, the cost of the gas storage systems is up to 0.11 €/kg. The CAPEX of PV and wind plants has a significant dependency on location and varies between 1.37 €/kg in the flexible system in the South of Italy and 2.16 €/kg in the inflexible system in the north of Italy. In Italy, the impact of the investment cost of the battery varies between 0.38 and 0.47 €/kg in flexible systems and increases up to 0.87–1.04 €/kg in inflexible systems. Credits associated to CO_2 capture and storage contribute to reducing the cost of hydrogen by 0.5 €/kg_{H2}. All the other OPEX contribute to the hydrogen cost by 2.16–2.67 €/kg.

As previously discussed, in the long-term scenario, the low cost of renewable power generation technologies and battery energy storage reduce the impact of plant flexibility and optimized flexible plants feature smaller oversizing of the chemical plant equipment as well as smaller gas storage units. This is the reason why the impact of the CAPEX of the chemical island in the flexible plant is only 0.71 €/kg (vs. 0.83 €/kg in the short-term scenario). The impact of the investment in renewables and battery varies between 0.81 and 1.14 €/kg in the flexible

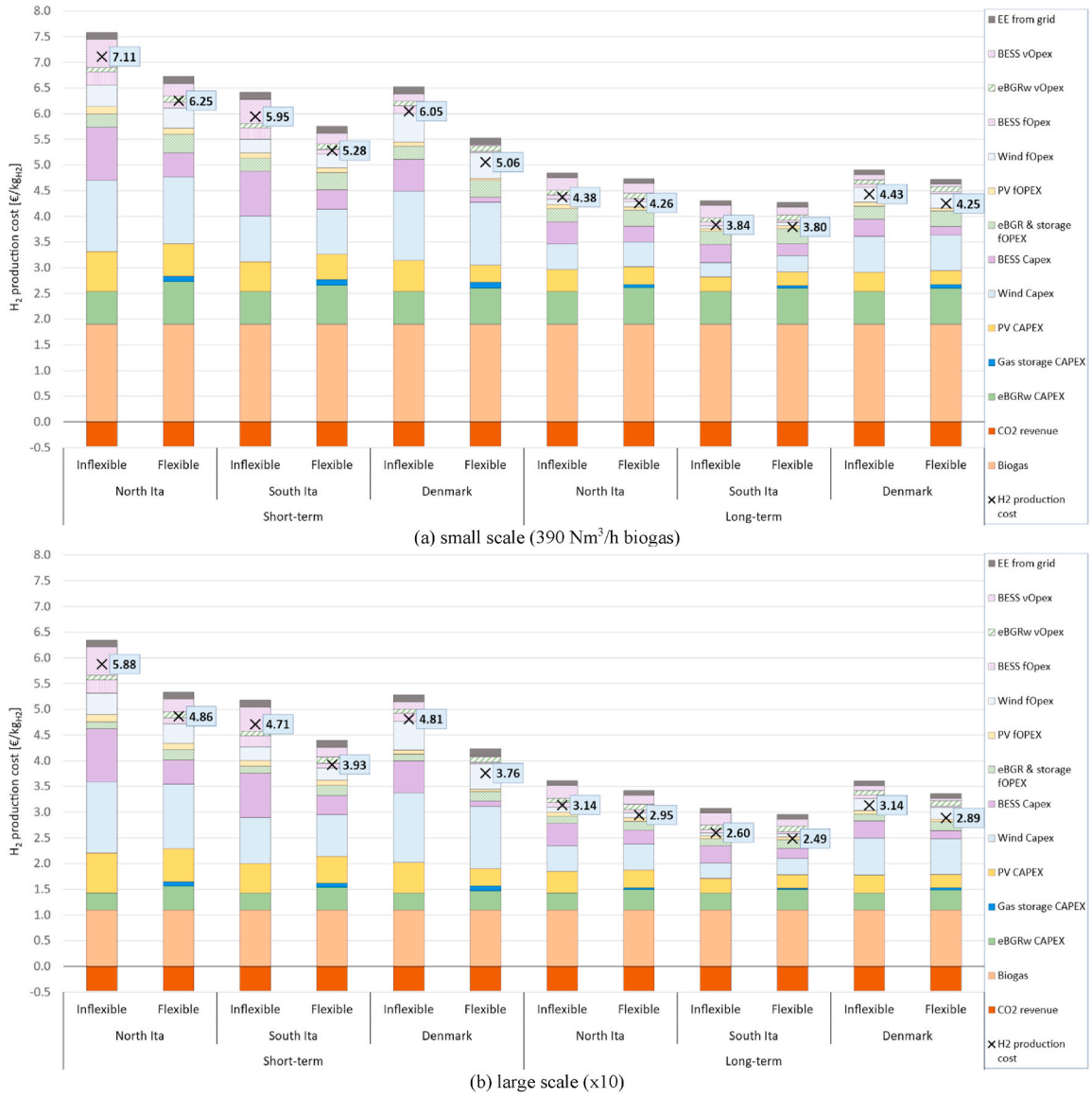

Fig. 12. Hydrogen production cost breakdown in (a) small-scale and (b) large-scale systems in both short-term and long-term scenarios with RENS = 95%.

cases and 0.91–1.40 €/kg in the inflexible ones. Overall, in the long-term scenario, the economic benefit of flexible plants reduces compared to the short-term scenario.

To investigate the scale-effect, a system fed with ten times the biogas flow rate (i.e., 3900 Nm^3/h) was assessed. According to IEA, large-scale biodigesters allow to reduce the cost of biogas production from 55 €/MWh to 32 €/MWh [3]. Moreover, the capital cost of the biogas to hydrogen plant reduce with size, thanks to the favourable scale-effect.

The results for large-scale systems are presented in Fig. 12b, with 95% renewable share. The impact of biogas on the cost of production decreases from 1.9 €/kg to 1.1 €/kg, while the impact of the chemical island drops from 0.64 to 0.83 €/kg to 0.33–0.41 €/kg. It is noteworthy that reducing the cost of the chemical island increases the benefits related to flexibility, and the cost difference between flexible and inflexible system increases accordingly. The cost of hydrogen is always lower in places with higher renewable availability and varies from 4.8 to 5.9 €/kg in inflexible plants to 3.8–4.9 €/kg with flexible plants, with a relative cost reduction of 17–23%, in the short-term scenario. In the long-term scenario, the cost of hydrogen is between 3.1 and 3.2 €/kg with inflexible plants and 2.5–2.9 €/kg with flexible plants, with a relative cost reduction ranging from 6 to 8% in the North Italy and Denmark cases to 22% in the South Italy case.

Table 5 reports the details of the main results of some interesting cases for flexible and inflexible systems in short and long term scenario and small and large scale plants.

4.2.3. Emissions

Fig. 13 shows the sources of equivalent CO_2 emissions for the flexible plants in North Italy for the minimum and maximum embedded CO_2 range reported in Table 2. In all cases, indirect emissions are lower than the captured CO_2, and therefore net emissions are always largely negative, and lower in places with higher renewable availability. The off-grid case has higher net emissions than the RENS = 95–99 % case, due to the oversized renewable capacity and the increasing curtailment. In flexible systems, reduced renewable and battery capacity leads to lower emissions for the same renewable share. The minimum values are achieved at RENS = 99% and are between −8.0 and −9.0 kg_{CO2}/kg_{H2}.

4.2.4. Comparison with electrolyser

This section presents a comparative analysis of the results obtained from the eBGR systems with an electrolyser producing the same amount of hydrogen. Fig. 14 illustrates the schematic of the electrolysis system,

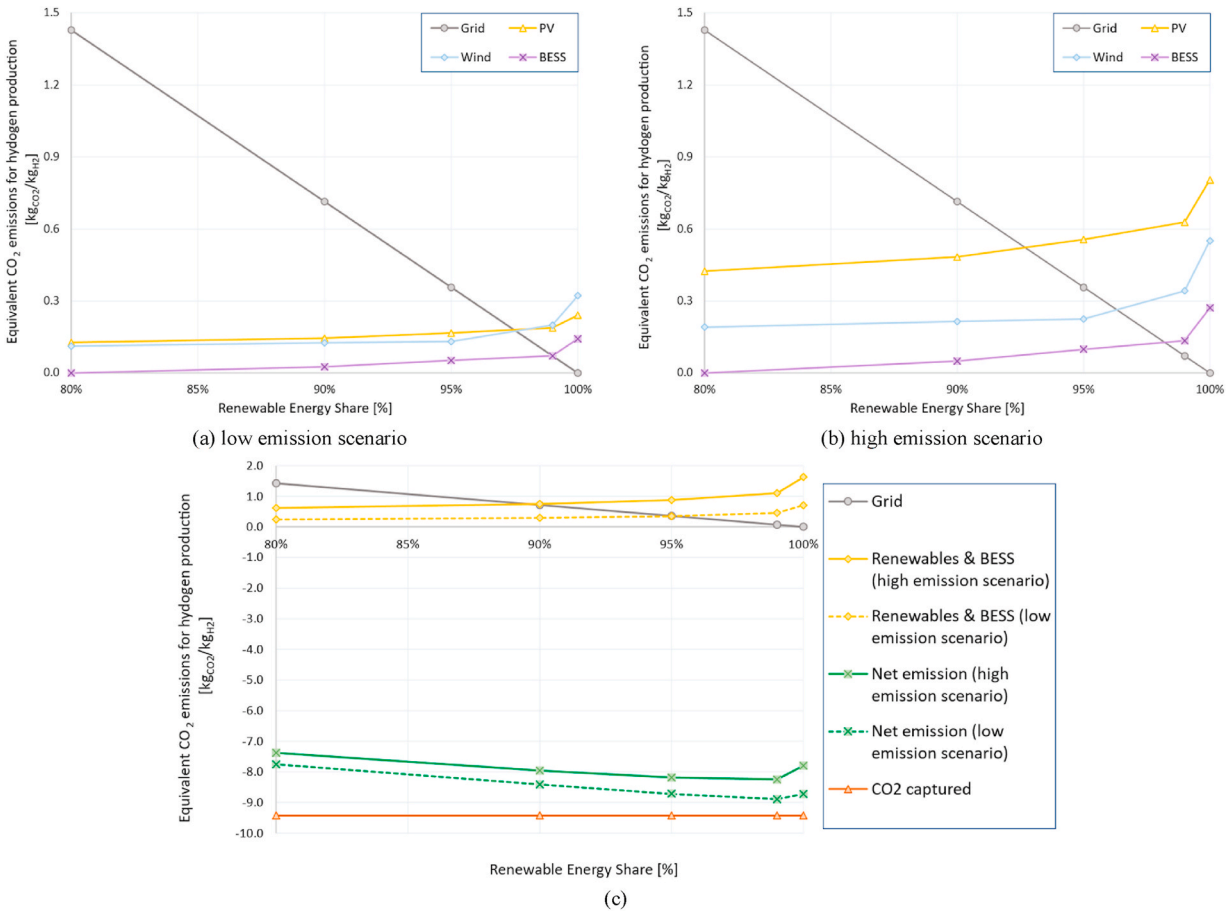

Fig. 13. Emissions from electricity grid and embedded emissions of renewables and battery in flexible system of north Italy, in the low emission (a) and high emission (b) scenarios. Total grid and renewable emissions, captured CO_2 and net emissions (c).

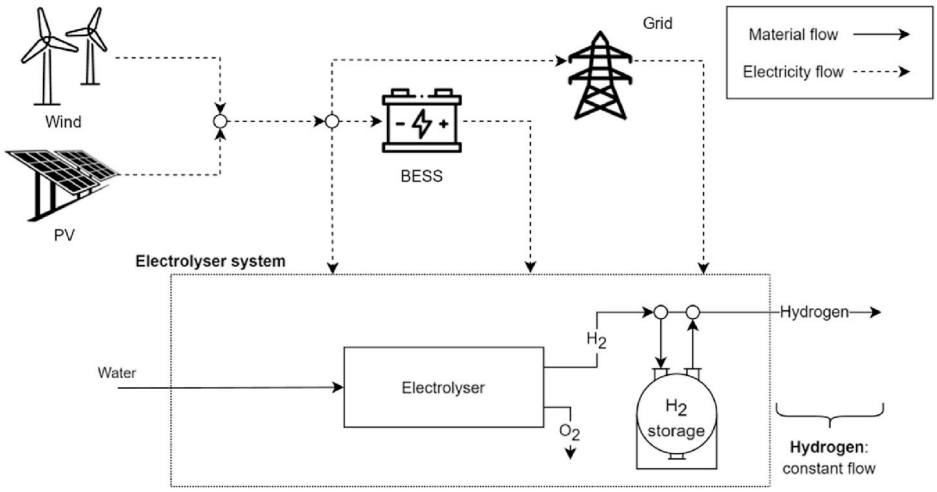

Fig. 14. Block scheme of the electrolyser system with power supply and hydrogen storage.

which includes the same power supply and hydrogen storage equipment as the previously analysed systems. The electrolyser can operate at partial load, with a minimum load of 5% of the maximum capacity. The capacity of the electrolyser, renewables and storage are optimization variables, and the system is simulated on an annual basis with hourly resolution. The technical and economic specifications of the electrolyser are listed in Table 2, while the assumptions for renewables and storage units are consistent with those used for the biogas-based systems.

Table 6 presents the results for the electrolysis systems, where it can be noted that electrolysers with a capacity of 5.5–9.9 MW are needed to produce the same amount of hydrogen of the small-scale eBGR plants. The size of the electrolyser is strongly influenced by the capacity factor of the renewable energy sources, and is larger in the case of North Italy. The electrolyser capacity factor is higher in Denmark due to the high availability of off-shore wind and is equal to 65% in the short-term scenario, compared to 38–44 % of the Italian cases.

Table 6
Results of electrolysis systems sized to produce the same hydrogen output as the small-scale eBGR plants.

Cost-scenario		short-term			long-term		
Location		North Ita	South Ita	Denmark	North Ita	South Ita	Denmark
Electrolyser capacity	MW	9.25	8.04	5.46	9.86	8.04	6.45
Electrolyser Capacity Factor	%	38%	44%	65%	31%	38%	47%
PV capacity	MW	15.25	12.42	–	19.41	13.42	10.96
Wind capacity	MW	8.21	4.93	6.82	0.20	2.23	3.56
BESS capacity	MWh	–	–	–	–	–	–
BESS eq. cycles	–	–	–	–	–	–	–
Hydrogen storage	m^3	1894	1449	3318	11,896	5492	6882
Hydrogen storage hours	h	66.4	50.8	116.4	417.3	192.6	241.4
$LCOE_{ren}$	€/MWh	104	73	80	36	30	64
EE curtailed	%	12%	9%	11%	12%	9%	4%
H_2 production cost	€/kg	10.16	8.01	7.80	2.98	2.49	3.89
REN $CO_{2,eq}$ emissions (low-/high-emission scenarios)	kg_{CO2}/kg_{H2}	0.82/2.36	0.62/1.84	0.19/0.33	0.82/2.63	0.59/1.85	0.52/1.59
Grid emission	kg_{CO2}/kg_{H2}	1.14	1.14	1.14	0.98	0.98	0.77
CO_2 capture	kg_{CO2}/kg_{H2}	–	–	–	–	–	–
Net emission (low-/high-emission scenarios)	kg_{CO2}/kg_{H2}	1.96/3.50	1.76/2.98	1.33/1.47	1.80/3.61	1.57/2.83	1.30/2.36

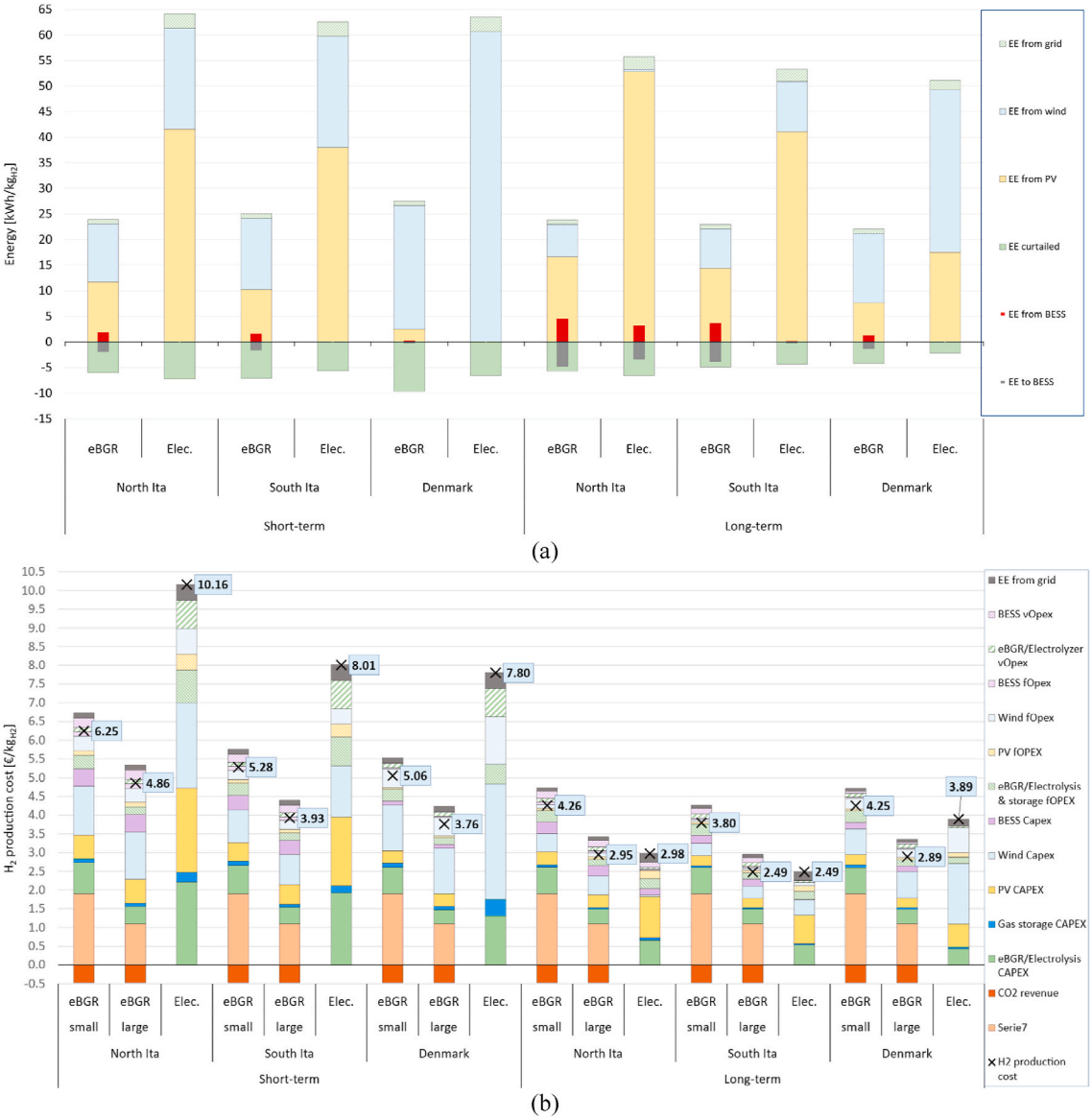

Fig. 15. Comparison between flexible eBGR and electrolysis systems: (a) annual energy balance breakdown and (b) hydrogen production cost breakdown. Results with RENS = 95%.

The energy required to produce 1 kg of hydrogen is significantly higher with an electrolyser than with electrified biogas reforming (49–57 kWh/kg_{H_2} in the long- and short-term scenario, respectively vs. 18 kWh/kg_{H_2}), resulting in higher annual energy flows, as illustrated in Fig. 15a.

In light of the considerable cost reduction for photovoltaics in the long-term, the optimal solution entails a greater installed capacity of PV and a reduced capacity of wind power, leading to an increased capacity of renewables and a reduced capacity factor of the electrolyser (31–38 % in Italy and 47 % in Denmark). In all cases, only 4–12 % of renewable energy is curtailed, vs. 19–36 % of the flexible eBGR plants. This is a consequence of the high flexibility of the electrolyser. Consequently, in order to guarantee a constant outflow of hydrogen from the system, the installation of substantially larger hydrogen storage unit is essential, as compared to those utilized in biogas systems (50–420 h vs. 3–18 h of storage).

The larger installed capacity of renewables has an impact on the hydrogen production cost, which is notably higher in the short-term scenario for the electrolysis than for eBGR systems, with a range of 7.8–10.2 €/kg_{H2}. The cost of green hydrogen is primarily influenced by the capital expenditure associated with the electrolyser (17–24 %) and renewable energy sources (39–44 %), as illustrated in Fig. 15b. By reducing the costs of these two key components, it is possible to lower the overall hydrogen production cost, which ranges from 2.5 to 3.9 €/kg_{H2} in the long-term scenario. This long-term cost is significantly lower than that of emerald hydrogen produced in small-scale eBGR plants and comparable to large-scale eBGR systems.

Emissions from electrolytic hydrogen production are always positive, as shown in Table 6. With RENS = 95 %, the emissions associated to grid electricity are found to be in the range of 0.8–1.1 kg_{CO2}/kg_{H2}, while the embedded emissions from renewables are in the range of 0.2–0.8 kg_{CO2}/kg_{H2} in the low emissions scenario and rise to 0.3–2.6 kg_{CO2}/kg_{H2} in the high emissions scenario. This leads to total emissions of 1.3–3.6 kg_{CO2}/kg_{H2}.

5. Conclusions

In this work, a biogas to hydrogen plant based on electrified steam methane reformer has been assessed. From process simulations, it was obtained that 96% of the biogas chemical energy (on LHV basis) can be retained in the hydrogen and 76% of the biogenic carbon is separated from the syngas and available for CO_2 capture and storage, leading to negative emission hydrogen production. The plant electrical consumption resulted 17.7 kWh/kg_{H2}, i.e. about three time less than the electric consumption of low temperature electrolysis.

The integration of the biogas to hydrogen plant with solar and wind power generation technologies has been assessed. The overall system has been optimized to minimize the levelized cost of hydrogen, based on yearly simulations with hourly resolution and considering: (i) inflexible and flexible biogas to hydrogen plants; (ii) three different European locations (South Italy, North Italy and Denmark), (iii) different shares of renewable electricity feeding the plant; (iv) short-term and long-term scenarios for the cost of photovoltaic and wind power generation and of battery energy storage system and (v) small-scale (390 Nm^3/h) biogas plant and large-scale (3900 Nm^3/h) plant. The following main conclusions result from the study.

- The levelized cost of hydrogen varies in a wide range depending on the case. For 95% renewable electricity share, in the different locations, it ranges from 2.5 to 2.9 €/kg for a long-term REN cost scenario and large-scale flexible plant to 5.9–7.1 €/kg for a short-term REN cost scenario and small-scale inflexible plants.
- The cost of renewable energy and the cost of biogas are the most impacting items on the cost of hydrogen. For 95% renewable energy share, renewable electricity and BESS contributes with 2.2–4.6 €/kg_{H2} in the short-term scenario and 1.1–1.9 €/kg_{H2} in the long-term scenario. The impact of the cost of biogas depends on the size of the plant and ranges between 1.9 €/kg_{H2} in small-scale plants and 1.1 €/kg_{H2} in large-scale plants.
- Adopting a flexible plant allows to reduce the renewable and battery capacity installed, as well as the amount of curtailed renewable electricity. This leads to a reduction in the hydrogen production cost of up to 11–16% with respect to the inflexible plant in case of 95% renewable energy share, for small-scale plants in a short-term cost scenario. The benefit of flexibility reduces in the long-term cost scenario, as the reduction of the cost of renewable technologies reduces the economic impact of REN oversizing, curtailment and electricity storage. In such scenario, the adoption of a flexible plant leads to a reduction of 1–4% of the hydrogen cost in case of 95% renewable energy share and small-scale plant. On the other hand, increasing the size of the plant leads to increased economic benefits of flexibility, thanks to the favourable scale effect on the capital cost of the chemical process equipment. In these cases, with 95% renewable energy share, the adoption of a flexible plant leads to a reduction of 17–23% of the hydrogen cost in the short-term scenario and of 6–22% in the long-term scenario.
- System emissions are always largely negative (−9 kg_{CO2}/kg_{H2}) if biogenic CO_2 is captured and stored. Cases with 95–99% RENS involve lower emissions than 100% RENS, mainly due to lower oversizing and the lower impact of the embedded emissions of REN technologies.
- Green hydrogen from electrolyser, compared to emerald hydrogen from biogas reforming with CCS requires more energy (i.e. 49 – 57 kWh/kg_{H2} vs 18 kWh/kg_{H2}) and consequently higher PV and wind capacity. The production cost is primarily driven by the investment in the electrolyser and renewables, resulting in a higher cost than that of emerald hydrogen in the short-term (7.8–10.2 €/kg_{H2} vs 5.1–6.2 €/kg_{H2}). Conversely, in the long-term scenario, electrolytic hydrogen is cheaper than emerald hydrogen produced in small-scale eBGR plants (2.5–3.9 €/kg_{H2} vs 3.8–4.3 €/kg_{H2}) and has comparable cost of large-scale eBGR systems (2.5–3.9 €/kg_{H2} vs 2.5–2.9 €/kg_{H2}).

Data availability statement

The data supporting the findings of this study, including all assumptions, methodologies used to simulate the plants on Aspen and GAMS, and all results, are provided in the main paper, supplementary information, and the GitHub repository “bio-H2-from-eSMR" at the following link: https://github.com/AndreaNava-Polimi/bio-H2-from-eSMR.git.

CRediT authorship contribution statement

Andrea Nava: Writing – original draft, Visualization, Software, Methodology, Investigation, Formal analysis, Conceptualization. **Davide Remondini:** Writing – review & editing, Supervision. **Stefano Campanari:** Writing – review & editing, Supervision, Funding acquisition. **Matteo C. Romano:** Writing – review & editing, Supervision, Methodology, Funding acquisition, Conceptualization.

Declaration of competing interest

The authors declare that they have no known competing financial interests or personal relationships that could have appeared to influence the work reported in this paper.

Acknowledgments

This study has been funded by SNAM SpA.

Appendix A. Supplementary data

Supplementary data to this article can be found online at https://doi.org/10.1016/j.ijhydene.2024.09.171.

References

[1] EBA. Biogenic CO2 from the biogas industry. 2022.
[2] EBA statistical report. European Biogas Association; 2023. n.d. https://www.europeanbiogas.eu/eba-statistical-report-2023/. [Accessed 30 January 2024].
[3] IEA. Sustainable supply potential and costs – outlook for biogas and biomethane: prospects for organic growth – analysis. IEA; 2020. https://www.iea.org/reports/outlook-for-biogas-and-biomethane-prospects-for-organic-growth/sustainable-supply-potential-and-costs.
[4] Poluzzi A, Guandalini G, d'Amore F, Romano MC. The potential of power and biomass-to-X systems in the decarbonization challenge: a critical review. Current Sustainable/Renewable Energy Reports 2021;8:242–52. https://doi.org/10.1007/S40518-021-00191-7/FIGURES/2.
[5] Wismann ST, Engbæk JS, Vendelbo SB, Bendixen FB, Eriksen WL, Aasberg-Petersen K, et al. Electrified methane reforming: a compact approach to greener industrial hydrogen production. Science 2019;364:756–9. https://doi.org/10.1126/SCIENCE.AAW8775/SUPPL_FILE/AAW8775-WISMANN-SM.PDF.
[6] Wismann ST. PhD thesis, electrically heated steam reforming reactor. Technical University of Denmark; 2019.
[7] Topsoe. eREACT^{TM} Hydrogen: the future of blue hydrogen | Equipment | Products | Topsoe. https://www.topsoe.com/our-resources/knowledge/our-products/equipment/ereact-hydrogen. [Accessed 18 June 2024].
[8] From TN, Partoon B, Rautenbach M, Østberg M, Bentien A, Aasberg-Petersen K, et al. Electrified steam methane reforming of biogas for sustainable syngas manufacturing and next-generation of plant design: a pilot plant study. Chem Eng J 2024;479:147205. https://doi.org/10.1016/J.CEJ.2023.147205.
[9] Balzarotti R, Ambrosetti M, Beretta A, Groppi G, Tronconi E. Investigation of packed conductive foams as a novel reactor configuration for methane steam reforming. Chem Eng J 2020;391:123494. https://doi.org/10.1016/j.cej.2019.123494.
[10] Zheng L, Ambrosetti M, Zaio F, Beretta A, Groppi G, Tronconi E. Direct electrification of Rh/Al2O3 washcoated SiSiC foams for methane steam reforming: an experimental and modelling study. Int J Hydrogen Energy 2023;48:14681–96. https://doi.org/10.1016/J.IJHYDENE.2022.12.346.
[11] Ferri G, Ambrosetti M, Beretta A, Groppi G, Tronconi E. Experimental investigation and 2D mathematical modelling of copper foams packed with Rh-Al2O3 catalysts for the intensification of methane steam reforming. Catal Today 2024;426:114386. https://doi.org/10.1016/J.CATTOD.2023.114386.
[12] Ambrosetti M, Beretta A, Groppi G, Romano MC, Tronconi E. Reactor with electrically heated thermo-conductive structure for endothermic catalytic process. WO 2023/062591 A1. 2023.
[13] Balakotaiah V, Ratnakar RR. Modular reactors with electrical resistance heating for hydrocarbon cracking and other endothermic reactions. AIChE J 2022;68:e17542. https://doi.org/10.1002/AIC.17542.
[14] Tiggeloven JL, Faaij APC, Kramer GJ, Gazzani M. Optimization of electric ethylene production: exploring the role of cracker flexibility, batteries, and renewable energy integration. Ind Eng Chem Res 2023;62:16360–82. https://doi.org/10.1021/ACS.IECR.3C02226/ASSET/IMAGES/LARGE/IE3C02226_0015.JPEG.
[15] Montenegro Camacho YS, Bensaid S, Piras G, Antonini M, Fino D. Techno-economic analysis of green hydrogen production from biogas autothermal reforming. Clean Technol Environ Policy 2017;19:1437–47. https://doi.org/10.1007/S10098-017-1341-1/TABLES/8.
[16] Crispim AM de C, Barros RM, Tiago Filho GL, dos Santos IFS. An economic study of hydrogen and ammonia generation from the reforming of biogas from co-digestion of municipal solid waste and wastewater sludge in a Brazilian state. Int J Hydrogen Energy 2024;67:312–26. https://doi.org/10.1016/J.IJHYDENE.2024.04.108.
[17] Keipi T, Tolvanen H, Konttinen J. Economic analysis of hydrogen production by methane thermal decomposition: comparison to competing technologies. Energy Convers Manag 2018;159:264–73. https://doi.org/10.1016/J.ENCONMAN.2017.12.063.
[18] Cormos CC, Cormos AM, Petrescu L, Dragan S. Techno-economic assessment of decarbonized biogas catalytic reforming for flexible hydrogen and power production. Appl Therm Eng 2022;207:118218. https://doi.org/10.1016/J.APPLTHERMALENG.2022.118218.
[19] Selejan AD, Lisei H, Cormos AM, Dragan S, Cormos CC. Development of a multi-scale mathematical model for green hydrogen production via biogas steam reforming process. Int J Hydrogen Energy 2024;52:469–84. https://doi.org/10.1016/J.IJHYDENE.2023.07.057.
[20] Madeira JGF, Oliveira EM, Springer MV, Cabral HL, Barbeito DF do C, Souza APG, et al. Hydrogen production from swine manure biogas via steam reforming of methane (SRM) and water gas shift (WGS): a ecological, technical, and economic analysis. Int J Hydrogen Energy 2021;46:8961–71. https://doi.org/10.1016/J.IJHYDENE.2021.01.015.
[21] Lachén J, Durán P, Menéndez M, Peña JA, Herguido J. Biogas to high purity hydrogen by methane dry reforming in TZFBR+MB and exhaustion by Steam-Iron Process. Techno–economic assessment. Int J Hydrogen Energy 2018;43:11663–75. https://doi.org/10.1016/J.IJHYDENE.2018.03.105.
[22] Ongis M, Di Marcoberardino G, Manzolini G, Gallucci F, Binotti M. Membrane reactors for green hydrogen production from biogas and biomethane: a techno-economic assessment. Int J Hydrogen Energy 2023;48:19580–95. https://doi.org/10.1016/J.IJHYDENE.2023.01.310.
[23] Maporti D, Nardi R, Guffanti S, Vianello C, Mocellin P, Pauletto G. Techno-economic analysis of electrified biogas reforming. Chem Eng Trans 2022;96:163–8. https://doi.org/10.3303/CET2296028.
[24] Grabke HJ. Metal dusting. Mater Corros 2003;54:736–46. https://doi.org/10.1002/MACO.200303729.
[25] Aspen Tech. Rate-based model of the CO2 capture process by MDEA using aspen Plus aspen Plus. 2008.
[26] Adams TA, Salkuyeh YK, Nease J. Processes and simulations for solvent-based CO2 capture and syngas cleanup. In: Reactor and process design in sustainable energy technology. Elsevier Inc.; 2014. p. 163–231. https://doi.org/10.1016/B978-0-444-59566-9.00006-5.
[27] Gas Processors Suppliers Association. Engineering data BOOK. 2004.
[28] Pfenninger S, Staffell I. Long-term patterns of European PV output using 30 years of validated hourly reanalysis and satellite data. Energy 2016;114:1251–65. https://doi.org/10.1016/j.energy.2016.08.060.
[29] IRENA. Electricity storage and renewables: costs and markets to 2030. 2017.
[30] Turton Richard, Bailie Richard C, Whiting Wallace B, Shaeiwitz JA. Analysis, synthesis, and design of chemical processes. Prentice Hall; 2012.
[31] Rath Lawrence K, Chou Vincent H, Kuehn NJ. Assessment of hydrogen production with CO2 capture volume 1: baseline state-of- the-art plants, vol. 1; 2010.
[32] Riva L, Martínez I, Martini M, Gallucci F, van Sint Annaland M, Romano MC. Techno-economic analysis of the Ca-Cu process integrated in hydrogen plants with CO2 capture. Int J Hydrogen Energy 2018;43:15720–38. https://doi.org/10.1016/j.ijhydene.2018.07.002.
[33] The Chemical Engineering Plant Cost Index ® - Chem Eng n.d. https://www.chemengonline.com/pci-home.
[34] IRENA. Renewable power generation costs in 2021. International Renewable Energy Agency 2022:160. Abu Dhabi. ISBN 978-92-9260-452-3. International Renewable Energy Agency 2022.
[35] Ram M, Galimova T, Bogdanov D, Fasihi M, Gulagi A, Breyer C, et al. POWERFUELS in a renewable energy world. 2020.
[36] Müller A, Friedrich L, Reichel C, Herceg S, Mittag M, Neuhaus DH. A comparative life cycle assessment of silicon PV modules: impact of module design, manufacturing location and inventory. Solar Energy Materials and Solar Cells. 2021;230:111277. https://doi.org/10.1016/J.SOLMAT.2021.111277.
[37] Kolahchian Tabrizi M, Famiglietti J, Bonalumi D, Campanari S. The carbon footprint of hydrogen produced with state-of-the-art photovoltaic electricity using life-cycle assessment methodology. Energies 2023;16:5190. https://doi.org/10.3390/EN16135190/S1.
[38] Schreiber A, Marx J, Zapp P. Comparative life cycle assessment of electricity generation by different wind turbine types. J Clean Prod 2019;233:561–72. https://doi.org/10.1016/J.JCLEPRO.2019.06.058.
[39] Cole W, Frazier AW, Augustine C. Cost projections for utility-scale battery storage : 2021 update. National Renewable Energy Lab; 2020. NREL/TP-6A20-79236, https://www.nrel.gov/docs/fy21osti/79236.pdf.
[40] Bonalumi D, Kolahchian Tabrizi M. Re-Evaluation of the global warming potential for the production of lithium-ion batteries with nickel-manganese-cobalt cathode chemistries in China. Energy and Fuels 2022;36:13753–67. https://doi.org/10.1021/ACS.ENERGYFUELS.2C02204/ASSET/IMAGES/MEDIUM/EF2C02204_0013.GIF.
[41] IRENA. Making the breakthrough: green hydrogen policies and technology costs. 2021.
[42] U.S. Department of Energy (DOE). Fuel cell technologies office multi-year research. Development, and Demonstration Plan - Section 3.3 Hydrogen Storage 2015.
[43] HyUnder. "Assessment of the potential, the actors and relevant business cases for large scale and seasonal storage of renewable electricity by hydrogen underground storage in Europe" Overview on all Known Underground Storage Technologies for Hydrogen Status: D(4) n.d.
[44] Apt J, Newcomer A, Lave LB, Douglas S, Dunn LM. An engineering-economic analysis of syngas storage. US Department of Energy's National Energy Technology Laboratory; 2008. p. 143.
[45] Turton R, Bailie RC, Whiting WB, Shaeiwitz JA. Analysis, synthesis, and design of chemical processes. Prentice Hall; 2012.
[46] Venkataraman S, Jakobi D. Advanced spun cast material for steam reformer furnace tubes, vol. 691. London, England: International Fertiliser Society Meeting; 2011. p. 20. 2011.
[47] National Engergy Technology Laboratory. Capital cost scaling methodology : revision 3 reports and prior. 2019. p. 1–49.
[48] Maher MJ, Williams HP. Model building in mathematical programming. Wiley; 2013. https://doi.org/10.2307/3009304.
[49] Zhao E, Walker PD, Surawski NC, Bennett NS. Assessing the life cycle cumulative energy demand and greenhouse gas emissions of lithium-ion batteries. J Energy Storage 2021;43:103193. https://doi.org/10.1016/J.EST.2021.103193.